Submitted to Physical Review

RECEIVED
LAWRENCE
RADIATION LABORATORY

LBL-34 c.2
Preprint

LIBRARY AND
DOCUMENTS SECTION

THE REACTIONS $K^- p \rightarrow \Lambda \pi^0$ AND $K^- p \rightarrow \bar{K}^0 n$ IN THE CENTER OF MASS ENERGY RANGE FROM 1700 TO 2100 MeV

A. J. Van Horn, R. P. Ely, and J. Louie

February 1972

AEC Contract No. W-7405-eng-48

TWO-WEEK LOAN COPY

This is a Library Circulating Copy which may be borrowed for two weeks. For a personal retention copy, call Tech. Info. Division, Ext. 5545

LBL-34 c.2

DISCLAIMER

This document was prepared as an account of work sponsored by the United States Government. While this document is believed to contain correct information, neither the United States Government nor any agency thereof, nor the Regents of the University of California, nor any of their employees, makes any warranty, express or implied, or assumes any legal responsibility for the accuracy, completeness, or usefulness of any information, apparatus, product, or process disclosed, or represents that its use would not infringe privately owned rights. Reference herein to any specific commercial product, process, or service by its trade name, trademark, manufacturer, or otherwise, does not necessarily constitute or imply its endorsement, recommendation, or favoring by the United States Government or any agency thereof, or the Regents of the University of California. The views and opinions of authors expressed herein do not necessarily state or reflect those of the United States Government or any agency thereof or the Regents of the University of California.

THE REACTIONS $K^-p \to \Lambda\pi^0$ AND $K^-p \to \bar{K}^0n$ IN THE CENTER OF MASS ENERGY RANGE FROM 1700 TO 2100 MeV*

A. J. Van Horn, R. P. Ely, and J. Louie†

E. O. Lawrence Berkeley Laboratory
University of California
Berkeley, California 94720

ABSTRACT

Cross-sections, angular distributions, and polarizations are presented for the reactions $K^-p \to \Lambda\pi^0$ and $K^-p \to \bar{K}^0n$ for 19 incident beam momenta in the center-of-mass energy range 1709 to 2106 MeV. Legendre polynomial expansion coefficients to seventh order are also given for the data. The experimental procedures and results from two exposures in the Lawrence Berkeley Laboratory 25" Hydrogen Bubble Chamber are discussed.

†Present address: CEN Saclay, 91 Gif-sur-Yvette, France.

I. INTRODUCTION

This paper presents new data for the reactions $K^-p \to \Lambda\pi^0$ and $K^-p \to \bar{K}^0n$ at 19 center of mass energies between 1709 and 2106 MeV with an average of about 0.8 events/microbarn at each energy. Several earlier experimental studies of these reactions may be found in the literature.[1] The data of this experiment are in an intermediate energy range which is rich in s-channel resonant structure. In particular our data span the region around 1900 MeV where the isospin one partial waves are notably ambiguous.[2] The reaction $K^-p \to \Lambda\pi^0$, a formation reaction which is pure isospin one, should be particularly revealing of this structure. Likewise, the charge exchange reaction $K^-p \to \bar{K}^0n$ can be used in conjunction with the elastic scattering measurements to determine the partial waves in this energy range.

This paper presents the experimental procedures and results from two exposures in the LBL 25" hydrogen bubble chamber. Cross sections, angular distributions and polarizations are presented for 19 incident beam momenta. The Legendre polynomial expansion coefficients are also given. The data are presented in a form which can be readily adapted for analysis, either alone or in conjunction with other experimental data.

A partial wave analysis of the first exposure is available in unpublished form in Ref. 3, and preliminary results for the second exposure were presented at the XVth International Conference on High Energy Physics at Kiev in 1970.[4] An analysis of the $\Sigma^+\pi^-$ and $\Sigma^-\pi^+$ final states has been published recently.[5] A complete analysis of the $\Lambda\pi^0$ final state is in progress and will be published shortly.

II. EXPERIMENTAL PROCEDURES

A. The K^- Beams and Normalization

A total of 1,093,000 pictures of K^-p interactions were taken in two separate exposures at the LBL 25" hydrogen bubble chamber. The first exposure covered the energy region from 1700 to 1850 MeV with nine incident K^- momenta, while the second spanned the range 1865 to 2106 MeV with 13 incident beam momenta (Fig. 1). Both exposures used two-stage electromagnetically separated beams produced by the external proton beam of the Bevatron. Details of the beam designs and parameters for the two beams are discussed elsewhere.[6] The beam was typically tuned to a momentum acceptance of ± 2% in the first exposure and ± 1% in the second, with a residual π^- plus μ^- contamination, determined by a δ ray count, of less than 10% at all momenta. The flux normalization for the first exposure was determined by a beam count and was checked by a tau scan ($K^- \to \pi^+\pi^-\pi^-$) in which the tau branching ratio was found to be consistent with the well-determined world average.[7] For the second exposure the normalization was based completely on the companion tau events.

B. Scanning, Measuring, and Kinematic Reconstruction

The event topology for the reactions $K^-p \to \Lambda\pi^0$ and $K^-p \to \bar{K}^0n$ as they appear in the bubble chamber is a vanishing beam track with a vee-like decay pointing to the production vertex (zero-prong + vee). The topology with two visible tracks at the production vertex plus a vee decay (two prongs + vee) was looked for in the same scan. A second scan was performed independently to determine the efficiency for finding event candidates. For the first exposure a complete second

scan was performed; for the second exposure about 16% of the film was double scanned. The initial scan had a mean efficiency of 93%; for double scanned film the combined efficiency was over 99%. A separate scan was also performed to find the three-prong tau decay mode of the K^- beam. Events found were measured on either the FSD (Flying Spot Digitizer) or the Franckenstein measuring machine under on-line computer control of the COBWEB system. Geometric and kinematic reconstruction of events was performed with the FOG-CLOUDY-FAIR analysis system. Events which were not well measured or failed to meet kinematic constraints were re-examined, and good event candidates were passed through the analysis system a second time.

The zero-prong + vee topology can result from the following reactions:

$$K^-p \rightarrow \Lambda\pi^0 \qquad (1)$$

$$\rightarrow \Lambda + \text{neutrals} \qquad (2)$$

$$\rightarrow \Sigma^0\pi^0 \qquad (3)$$

$$\rightarrow \Sigma^0 + \text{neutrals} \qquad (4)$$

$$\rightarrow \bar{K}^0 n \qquad (5)$$

$$\rightarrow \bar{K}^0 + \text{neutrals} \qquad (6)$$

The vee was fit kinematically to both the $\bar{K}^0$ and Λ^0 hypotheses; the fit having one-constraint when only the decay tracks are fit, or three-constraints when the position of the production vertex is included. The complete reaction hypothesis was then kinematically fit using the production and decay vertex positions, the two decay tracks, and a momentum edited beam track as the input information. The missing neutral momentum makes this a four constraint fit. Event candidates which

would not constrain in the 1c or 3c fits but which otherwise met our scanning and measurement acceptance criteria were accounted for in the reaction cross sections but were not included in the sample for analysis

C. Final State Selection

1. Separation of Lambdas and K-Zeros

The K^o and the Λ decays can be kinematically ambiguous when the laboratory momenta and the opening angle of the decay products are identical for the two hypotheses. In the Λ and K^o rest frames the decay momenta are 100 and 206 MeV/c, respectively. Thus in order to be ambiguous, events are restricted to having a maximum decay momentum component of 100 MeV/c perpendicular to the laboratory direction of the K^o. This restriction and the limitation that the Λ is always produced forward in the laboratory at our beam energies require for ambiguous events that the decay cosine of the π^+ in the K^o rest frame $\cos\beta = (\hat{p}_{\pi^+} \cdot \hat{p}_{K^o})$ be greater than + .87. Measurement uncertainties broaden this region of ambiguity, but we can select such events to be examined for ionization. In practice, events which constrained only as lambdas in the 4c fit did not require examination. The identification of the ambiguous decay particle was resolved by ionization when the laboratory momentum of the positive decay track (π^+ or p) was below $\approx$ 1.5 GeV/c. About 8% of the events were identified in this manner, with the remainder being distinguishable by kinematics. From a study of the resulting distribution of $\cos\beta$ it is estimated that less than 1% of the K^o sample were mis-identified as lambdas.

2. Missing Mass Selection

Once the vees are identified, we must distinguish among reactions (1) - (4) for lambdas, and between reactions (5) and (6) for K-zeros. This was done from a study of the missing mass squared spectrum, $(MM)^2$, to the Λ or K^o at the production vertex:

$$K^- p \rightarrow \Lambda + (MM) \quad \text{or}$$
$$K^- p \rightarrow \bar{K}^o + (MM).$$

The distributions of missing mass squared are shown for all incident momenta combined in Figs. 2 and 3. These distributions were calculated using the $\Lambda(K^o)$ momentum from the 1c fit and the edited beam momentum for the event. Due to experimental resolution the π^o line width has been broadened to about $\pm$ .02 GeV^2, and the neutron line width to about $\pm$ .035 GeV^2. Lambda events with $(MM)^2 = .018 \pm .05 GeV^2$ were included in the $\Lambda\pi^o$ sample and K^o events with $(MM)^2 = .882 \pm .20$ GeV^2 in the $\bar{K}^o n$ sample. These cuts effectively eliminate multiple π^o states. This selection gives a clean sample of $\bar{K}^o n$ events; however, for $\Lambda\pi^o$ events the sample suffers from contamination from reaction (3), as well as from a correctable kinematic bias.

a. Σ^o Contamination

The $(MM)^2$ spectrum for the $\Sigma^o\pi^o$ final state is flat because the spin of the Σ is 1/2. This distribution starts just above $(MM)^2 \simeq m^2_{\pi^o}$ and extends up to a value dependent on the c.m. energy. For example, for an incident K^- of 1 BeV/c, $(MM)^2_{max} \simeq 0.27$ GeV^2. From cross sections determined in this same experiment,[5] we estimated the maximum $\Sigma^o\pi^o$ cross section using the isospin relation

$$\sigma(\Sigma^o\pi^o) \leq \frac{1}{4}\left[\sqrt{\sigma_{\Sigma^-\pi^+}} + \sqrt{\sigma_{\Sigma^+\pi^-}}\right]^2$$

Given our experimental resolution, the maximum possible contamination for any momentum is 7%, and after all selection criteria the average contamination is about 5%. We have accounted for this in calculating $\Lambda\pi^o$ cross sections, but these events remain in our angular distributions.

b. Kinematic Bias of MM Selection

Two possible criteria were available for selecting the final state: a missing mass cut and a four constraint kinematic chi-squared cut. A minimum χ^2 requirement is not sufficient since an event with a large $(MM)^2$ would pass the χ^2 criteria if the errors were also large. Thus we cut on missing mass, but it can be shown that the error in $(MM)^2$ increases with increasing lambda momentum. A $(MM)^2$ cut then selectively excludes fast lambdas from our sample, biasing our angular distributions. We can correct for this by weighting events depending on their error in $(MM)^2$ (see section D4). This bias is not present for the K^o events because of the wider interval used in the missing mass selection.

To obtain the final sample of events we also applied a $\chi^2 \leq 10$ cutoff for the 1c fit to the vee decay tracks to insure well-constrained events. Events with $\chi^2 > 10$ were preferentially events where one of the decay tracks was nearly parallel to a camera axis and thus was difficult to measure and constrain. After applying these selection criteria, the results of the 4c fit with the missing neutral constrained to be a π^o or neutron were used. The 1c fit results were used only for the 3% of the selected events which failed to constrain in the two vertex

fit.

D. Weighting of Events

Our data sample is limited by bubble chamber detection characteristics as well as by our selection criteria. To obtain a consistent sample at each beam momentum and to insure uniform normalization, it was necessary to make cuts in the chamber volume and beam phase space. We have corrected our biases by weighting events according to the inverse of their detection and selection probabilities.

1. Lifetime Weight

Within the fiducial volume the probability for a decay with length $L_o < L < L_p$ is:

$$W_L^{-1} = \exp(-L_o/d) - \exp(-L_p/d),$$

where L_o is the minimum decay length cutoff, L_p is the potential path length within our cylindrical fiducial volume for a $\Lambda(K^o)$ of given direction, $d = \eta c\tau$ is the mean decay length for a particular $\Lambda(K^o)$, where $\eta = |p|/m$, p is the momentum, c is the velocity of light, and τ is the proper lifetime. A minimum decay length cut of 4 mm in the chamber has been applied to insure that short lambdas or K-zeros were not missed by our scanners.

The average weight, W_L, for the detection probability with the minimum length cutoff was 1.19 for both lambdas and K-zeros.

2. Momentum Dependent Weight for K-Zeros

There are two sources of events lost from the K-zero sample due to scanning bias. When the opening angle between the K^o decay products approaches 180° in the laboratory, it is likely the vee is not seen

by the scanner or is mistaken for a background track with a slight kink. A few forward K^o are also missed due to short pion tracks (less than 2%). Since vees mistaken for background tracks constitute the principal loss, we must use an empirical correction to account for these events. Both losses contribute to an anisotropic distribution of $\cos\beta = (\hat{p}_{\pi^+} \cdot \hat{p}_{K^o})$. The deviation from isotropy measures the fraction of K^os lost. We independently estimated the number of events lost by comparing the momentum distributions of the π^+ and π^- which should be identical but are not because of this scanning discrimination. A weight dependent on the laboratory production angle is assigned to account for these events. The effect of this weight on the production center of mass angular distribution $\cos\theta_1 = (\hat{p}_{K^o} \cdot \hat{p}_{K^-})$ was predominantly near $\cos\theta_1 \approx -1$, where the average weight assigned was 1.10. The average weight across the angular distribution was 1.04.

3. Short Decay Tracks Weight for Lambdas

A scanning bias against short decay tracks caused the isotropic decay distribution of the cosine of the angle between the proton in the lambda rest frame and the lambda direction to be depleted at both ends, i.e. near $\cos\beta' = (\hat{p}_p \cdot \hat{p}_\Lambda) \approx \pm 1$. By applying a minimum range (momentum) cutoff to both the decay pion and proton we can account for these missed events. Each accepted event is given a weight

$$W_p = \frac{2}{(1 - \cos\delta)}, \quad \cos\delta = (\hat{p} \cdot \hat{p}_\Lambda)$$

where $\hat{p}$ is a unit vector representing the minimum momentum proton or pion translated to the Λ rest frame and $\hat{p}_\Lambda$ denotes the Λ direction.

Maximizing both the total weighted events and the ratio of unweighted to weighted events determined the minimum consistently observable momentum for the proton as 0.160 GeV/c (range ~ 1.6 cm) and for the pion as 0.047 GeV/c (2.6 cm). For $0.1 < p_\Lambda < 0.4$ GeV/c, $\langle W_p \rangle = 1.16$, and for all p_Λ $\langle W_p \rangle = 1.06$.

4. Missing Mass Resolution Weight

This weight is related to our $(MM)^2$ selection for $\Lambda\pi^o$ events. It is negligible for $\bar{K}^o n$ events because of the relatively broader interval in $(MM)^2$ selected for those events. By choosing an interval of $(MM)^2$ we excluded events which were real $\Lambda\pi^o$ events but lay outside the interval, due to a large propagated error in $(MM)^2$. Because this error increases with increasing Λ momentum, we have excluded fast Λ's with our $(MM)^2$ cuts. To avoid a bias we weight each event within the chosen interval by $W_m = P_m^{-1}$, where P_m is the probability that a given $(MM)^2$ will be within the interval. For Gaussian distributed physical measurements, the probability for $(MM)^2$ to be within the interval defined by $|(MM)^2 - m_{\pi^o}^2| \leq \Delta$ is given by

$$P_m = \frac{1}{\sqrt{2\pi\sigma^2}} \int_{m_{\pi^o}^2 - \Delta}^{m_{\pi^o}^2 + \Delta} \exp\left\{ \frac{-(m^2 - m_{\pi^o}^2)^2}{2\sigma^2} \right\} dm^2$$

where σ is the propagated error in $(MM)^2$. We set $\Delta = 0.05$, so our interval remains below the two π^o threshold. The effect of this weight is predominantly at negative $\cos\theta_2 = (\hat{p}_{\pi^o} \cdot \hat{p}_{K^-})$ in the production center of mass. In the backward direction the average value of this weight is $\langle W_m \rangle = 1.54$ and for all cm angles $\langle W_m \rangle = 1.16$. This weight

accounts for events which are excluded by the $(MM)^2$ cut from the distribution of cos β' and from the distribution of the azimuthal production angle of the lambda about the beam direction. The latter distribution should be uniform for an unpolarized target, but is depleted by the $(MM)^2$ cuts due to larger measurement error on events moving away from the cameras.

After applying all selection criteria and multiplying the respective weights for each event, the data sample for $K^- p \rightarrow \Lambda\pi^0$ included 8256 unweighted events with an average weight per event of 1.46, and the sample for $K^- p \rightarrow \bar{K}^0 n$ consisted of 9119 unweighted events with an average weight of 1.28. The effects of the weighting on the combined angular distributions may be seen in Fig. 4.

III. EXPERIMENTAL RESULTS

A. Reaction Cross Sections

The cross sections and normalizations for the twenty-one incident beam momenta are presented in Table I. The cross section is given by

$$\sigma(\text{mb}) = \frac{\text{number of events}}{\rho\ NL}$$

where ρ = density of hydrogen; N = number of protons/gmH_2; and L = total K^- pathlength in the fiducial volume corrected for attenuation due to decay and interaction. Our calculations are based on a mean K^- decay length of 3.70 meters, a hydrogen density of .06014 gm/cm^3, a visible Λ decay fraction of .653, a visible K^0 decay fraction of .687, a ratio K^0_S/K^0_L = 1.0, and a τ decay branching ratio of .0557.[7] The cross sections include corrections for scanning

efficiencies and kinematic fitting throughput efficiencies. The error quoted is an error determined by adding in quadrature the uncertainties in total pathlength and efficiencies, and the statistical uncertainty in the number of events.

B. Angular Distributions and Polarizations

The angular distributions for 19 center-of-mass energies are presented in twenty equal bins of $\cos\theta = (\hat{p}_{meson} \cdot \hat{p}_{K^-})$. See Tables II and III. In two cases data from adjacent beam momenta have been combined to give greater statistical reliability. Both weighted and unweighted numbers of events are given. The sums of the polarization cosines for the lambdas are presented in twenty equal bins of $\cos\theta$ in Table IV. The polarization in a bin is $P = (3 \sum_i \cos \chi_i)/\alpha N$, where N = number of unweighted events in the bin; $\alpha = 0.645$, the parity violating lambda decay asymmetry parameter; $\cos \chi_i = (\hat{p}_i \cdot \hat{n}_i)$, $\hat{p}_i$ is a unit vector parallel to the proton in the Λ rest frame, and $\hat{n}_i$ is a unit vector normal to the production plane $(\hat{n} = (\hat{K}^- \times \hat{\pi}^o)/|\hat{K}^- \times \hat{\pi}^o|)$.

The error in the polarization is given by

$$\Delta P = \sqrt{\frac{3 - Q}{\alpha^2 N}}$$

where Q is either $(\alpha P)^2$ or 1.0, whichever is smaller. The angular distributions and polarizations are plotted in Figs. 5-7.

C. Legendre Coefficients

Each production angular distribution has been normalized to the cross section and expanded in the Legendre series.

$$\frac{d\sigma}{d\Omega} = \lambda\!\!\!^{-2} \sum_n A_n P_n \ (\cos\theta)$$

where $2\pi\lambda\!\!\!^{-}$ is the center-of-mass wavelength of the K^- and $A_o = \frac{\sigma}{4\pi\,\lambda\!\!\!^{-2}}$. The polarization distributions have been expanded in the first associated Legendre polynomial series

$$\vec{P}\ \frac{d\sigma}{d\Omega} = \lambda\!\!\!^{-2}\hat{n} \sum_n B_n P_n^{\ 1} \ (\cos\theta).$$

In the determination of the coefficients adjacent bins were combined by a computer algorithm to maintain a minimum of 6 events/bin in the angular distributions and about 40 events/bin in the polarizations. The Legendre coefficients up to ninth order were then determined by a chi-squared minimization requiring simple matrix inversion. Coefficients of higher than seventh order were entirely consistent with zero and did not significantly increase the fit probability at any momentum. The coefficients fit to sixth or seventh order, as indicated, are tabulated in Tables V - VII, and plotted in Figs. 8-10.

D. Lambda Lifetime

The value of the Λ lifetime was calculated for events in the first eight energies using the Bartlett method.[8] A corrected production vertex was determined by extending the beam track and Λ directions and finding the point of closest approach. This was necessary because the measured position of the last bubble on the beam track does not usually coincide with the production vertex. For 3950 events $\tau = (2.51 \pm 0.05) \times 10^{-10}$ sec., in excellent agreement with the world average.[7]

IV. DISCUSSION

With a few exceptions the data of this experiment are consistent with the data of Ref. 1. Representative differences in the reaction cross sections may be seen by comparing the A_0 Legendre coefficients plotted in Figs. 8 and 10. The Legendre coefficients for the angular distributions and polarization distributions are generally within the statistical error of other experimental coefficients. Where differences occur the limited statistics of the distributions make a preference difficult.

The new $\Lambda\pi^0$ data increases by about a factor of two the world's present data for this reaction between 1800 and 2000 MeV. This data should help to clarify the existence and properties of the P_{11} $\Sigma(1880)$, F_{15} $\Sigma(1915)$, and D_{13} $\Sigma(1940)$ seen in partial wave analyses.[2] The new charge exchange data will make possible a more complete analysis of the $\bar{K}N$ elastic channel. These analyses can then be used to test the several models of strong interactions which apply to these reactions.

ACKNOWLEDGMENTS

The authors would like to thank the crews of the LBL Bevatron and 25" Bubble Chamber, the scanners and support personnel of the Birge Physics Group, and members of the Data Handling Group for their assistance in this experiment. We would also like to thank Dr. Robert Birge and Dr. Daniel Kane for their aid during much of the experiment.

FOOTNOTES AND REFERENCES

*Work done under the auspices of the U.S. Atomic Energy Commission.

1. For example:

(a) R. Armenteros, M. Ferro-Luzzi, D. W. G. S. Leith, R. Levi Setti, A. Minten, R. D. Tripp, H. Filthuth, V. Hepp, E. Kluge, H. Schneider, R. Barloutaud, P. Granet, J. Meyer, and J. P. Porte, Nuclear Physics B8, 233 (1968).

(b) C. G. Wohl, F. T. Solmitz, and M. L. Stevenson, Phys. Rev. Letters 17, 107 (1966).

(c) A. Berthon, L. K. Rangan, J. Vrana, I. Butterworth, P. J. Litchfield, A. M. Segar, J. R. Smith, J. Meyer, E. Pauli, and B. Tallini, Nuclear Physics B20, 476 (1970).

(d) C. Bricman, M. Ferro-Luzzi, J. M. Perreau, G. Bizard, Y. Declais, J. Duchon, J. Seguinot, G. Valladas, Physics Letters 31B, 148 (1970). This was a counter experiment which measured the charge-exchange cross section. All other experiments referred to are bubble chamber experiments.

(e) P. J. Litchfield, T. C. Bacon, I. Butterworth, J. R. Smith, E. Lesquoy, R. Strub, A. Berthon, J. Vrana, J. Meyer, E. Pauli, B. Tallini, and J. Zatz, Nuclear Physics B30, 125 (1971).

2. (a) W. M. Smart, Phys. Rev. 169, 1330 (1970).

(b) P. J. Litchfield, Nuclear Physics B22, 269 (1970).

(c) R. Armenteros, P. Baillon, C. Bricman, M. Ferro-Luzzi, E. Pagiola, J. O. Petersen, D. E. Plane, E. Burkhardt, H. Filthuth, E. Kluge, and H. Oberlack, The $\bar{K}N$ Interaction Between 400 and 1200 MeV/c: First Attempt to an Energy Independent

Partial Wave Analysis in the $\bar{K}N$, $\Sigma\pi$ and $\Lambda\pi$ Channels, in Proceedings of Duke Conference on Hyperon Resonances (Moore Publishing Company, Durham, North Carolina, 1970), p. 123.

(d) Angela Barbaro-Galtieri, Review of Partial-Wave Analyses of the $\bar{K}N$ System Above 1.1 GeV/c K^- Beam Momentum, in Ref. 2c, p. 173.

(e) P. J. Litchfield, Ref. 1e, p. 134.

(f) R. Armenteros et al., Nuclear Physics B8, 183 (1968).

3. J. Louie, Exchange Amplitude Contributions to the Reaction $K^-p \to \Lambda\pi^0$ Near 1 BeV/c (Ph.D. Thesis) UCRL-18411, August 1968 (unpublished).

4. R. P. Ely, R. W. Birge, J. Hoven, G. E. Kalmus, D. Kane, and A. Van Horn, Study of the $\Sigma(1915)$ Resonance in the Reaction $K^-p \to \Lambda\pi^0$, UCRL-19789, August 1970.

5. D. Kane, Partial Wave Analysis of $K^-p \to \pi^{\pm}\Sigma^{\mp}$ Between 1.73 and 2.11 GeV, LBL-15, July 1971 (to be published in Physical Review).

6. (a) R. B. Bell et al., A Variable Momentum Separated K^+ Beam at the Bevatron, in Proceedings of the XIIth International Conference on High Energy Physics, Dubna, 1964. (Atomizdat, Moscow, 1966). Vol. I, p. 546.

(b) John A. Kadyk, K67 Beam, Trilling-Goldhaber Group (LRL) Technical Notes 122 and 124, January 1967.

(c) D. Kane, Modification of K67 Beam for Momenta Between 1.0 and 2.0 BeV/c, Powell-Birge Group (LRL) Physics Note 123, February 1968.

(d) A. Van Horn, Manual for LRL Separated πKp Beam, Powell-Birge Group (LRL) Physics Note 130, September 1968.

7. Particle Data Group, Review of Particle Properties, Physics Letters 33B, 1 (1970).

8. (a) M. S. Bartlett, Statistical Estimation of Mean Lifetimes, Philosophy Magazine 44, 249 (1953).

(b) J. Louie, Lambda Lifetime and Bartlett S-Function Technique, Powell-Birge Group (LRL) Technical Note 104, December 1966.

Table I. Reaction Cross Sections and Normalizations

P_{LAB} (GeV/c)	$E_{c.m.}$ (GeV)	K^- Path length* (μb/event)	Cross Section $\Lambda\pi^0$ (mb)	Cross Section $\bar{K}^0 n$ (mb)
.821	1.709	9.97 ± .50	2.75 ± .29	4.15 ± .47
.882	1.738	2.87 ± .10	3.09 ± .19	4.52 ± .30
.924	1.758	1.50 ± .08	3.15 ± .21	5.17 ± .34
.943	1.767	9.14 ± .46	3.82 ± .35	5.74 ± .56
.975	1.782	1.40 ± .07	3.21 ± .20	5.64 ± .35
1.020	1.803	1.27 ± .06	2.66 ± .16	6.64 ± .38
1.058	1.821	3.13 ± .16	2.48 ± .19	8.46 ± .56
1.112	1.846	3.74 ± .19	1.86 ± .16	6.36 ± .46
1.153	1.865	2.32 ± .10	1.78 ± .14	4.24 ± .31
1.190	1.882	2.39 ± .11	1.62 ± .13	3.82 ± .30
1.208	1.890	1.48 ± .06	1.50 ± .10	3.49 ± .23
1.262	1.915	2.11 ± .10	1.32 ± .12	2.10 ± .19
1.278	1.922	1.73 ± .07	1.32 ± .10	2.06 ± .17
1.310	1.937	1.16 ± .04	1.33 ± .09	1.69 ± .12
1.345	1.953	1.97 ± .09	1.23 ± .10	1.73 ± .15
1.384	1.970	2.05 ± .09	1.34 ± .12	1.60 ± .15
1.453	2.001	1.09 ± .04	1.27 ± .09	2.26 ± .16
1.500	2.022	1.63 ± .07	1.15 ± .10	2.16 ± .17
1.567	2.051	1.87 ± .08	1.10 ± .10	1.80 ± .16
1.644	2.085	1.84 ± .08	1.08 ± .10	2.14 ± .18
1.694	2.106	1.26 ± .05	.82 ± .07	1.71 ± .13

*Error combines statistical uncertainty, uncertainty in momentum, and uncertainties in tau efficiencies.

Table II. Unnormalized angular distributions for $K^- p \rightarrow \Lambda \pi^0$ in twenty equal bins of cos θ.

NUMBER WEIGHTED / NUMBER UNWEIGHTED

CENTER	1.709 GeV	1.738 GeV	1.758 GeV	1.767 GeV	1.782 GeV	1.803 GeV	1.821 GeV	1.846 GeV
-.95	13.0/ 9	98.5/ 62	158.1/100	23.3/ 14	116.9/ 69	107.6/ 60	33.9/ 21	10.6/ 7
-.85	18.0/ 12	65.5/ 46	105.1/ 65	31.8/ 22	104.2/ 68	95.5/ 53	30.3/ 16	19.4/ 8
-.75	6.6/ 5	42.1/ 31	106.2/ 69	22.3/ 14	99.9/ 59	69.1/ 42	25.4/ 14	19.5/ 12
-.65	12.0/ 9	55.0/ 39	82.3/ 49	14.7/ 10	72.5/ 43	80.6/ 54	31.9/ 18	9.6/ 6
-.55	9.9/ 8	38.9/ 27	74.6/ 47	17.8/ 12	65.1/ 39	62.3/ 40	18.8/ 10	6.0/ 3
-.45	10.8/ 7	27.6/ 19	54.0/ 39	9.0/ 7	60.8/ 37	34.2/ 24	17.5/ 12	8.8/ 6
-.35	10.3/ 6	26.3/ 19	43.6/ 30	8.8/ 7	49.0/ 34	30.1/ 21	9.7/ 6	11.6/ 6
-.25	9.0/ 7	24.0/ 18	57.4/ 42	7.5/ 6	49.4/ 34	43.8/ 31	15.7/ 8	7.6/ 5
-.15	7.5/ 5	17.3/ 13	44.0/ 32	6.5/ 5	44.9/ 33	45.1/ 31	16.3/ 10	5.1/ 3
-.05	2.3/ 2	18.0/ 14	43.0/ 32	10.3/ 8	48.5/ 36	34.8/ 23	11.3/ 8	2.8/ 2
+.05	1.3/ 1	11.0/ 9	26.9/ 21	10.3/ 8	48.2/ 37	32.6/ 24	14.5/ 11	12.7/ 8
+.15	1.2/ 1	15.1/ 12	24.4/ 18	5.4/ 4	42.0/ 31	34.7/ 27	15.3/ 12	10.4/ 7
+.25	3.7/ 3	1.6/ 1	26.0/ 20	6.5/ 5	53.1/ 39	43.7/ 33	22.2/ 17	11.7/ 9
+.35	1.2/ 1	3.6/ 3	23.6/ 18	4.8/ 4	48.4/ 36	56.2/ 44	30.5/ 24	9.3/ 7
+.45	2.4/ 2	12.8/ 10	16.6/ 13	3.6/ 3	54.5/ 44	52.0/ 41	20.7/ 17	21.2/ 17
+.55	1.2/ 1	11.0/ 9	41.5/ 34	4.9/ 4	49.9/ 40	84.1/ 67	27.0/ 22	19.2/ 15
+.65	11.0/ 9	25.4/ 21	53.5/ 43	7.9/ 6	62.2/ 51	74.9/ 61	42.8/ 35	33.7/ 27
+.75	11.0/ 9	34.5/ 29	61.0/ 51	16.7/ 14	64.4/ 54	65.9/ 55	39.7/ 33	25.1/ 21
+.85	18.4/ 14	58.1/ 45	110.8/ 87	15.0/ 12	107.3/ 87	94.6/ 78	40.6/ 33	37.0/ 31
+.95	27.0/ 12	98.2/ 45	170.9/ 91	41.4/ 21	203.7/ 99	162.7/ 90	41.5/ 25	28.4/ 17
TOTAL	177.9/125	684.6/472	1323.4/901	268.6/186	1444.8/970	1304.5/899	505.6/352	309.7/217

NUMBER WEIGHTED / NUMBER UNWEIGHTED

CENTER	1.865 GeV	1.887 GeV	1.919 GeV	1.937 GeV	1.953 GeV	1.970 GeV	2.001 GeV	2.022 GeV
-.95	12.4/ 6	39.7/ 27	46.5/ 20	57.0/ 26	23.1/ 11	21.2/ 11	36.0/ 20	22.4/ 10
-.85	13.2/ 7	32.7/ 24	34.6/ 16	22.9/ 11	4.6/ 3	14.5/ 6	17.2/ 9	13.2/ 8
-.75	24.1/ 15	36.3/ 23	29.2/ 17	5.4/ 4	10.6/ 6	10.7/ 5	17.2/ 10	12.0/ 6
-.65	12.3/ 9	23.1/ 15	26.9/ 17	25.6/ 17	15.6/ 8	26.1/ 11	16.3/ 8	18.4/ 10
-.55	10.8/ 8	16.0/ 12	12.3/ 9	20.8/ 11	8.8/ 6	19.6/ 12	37.9/ 24	16.9/ 10
-.45	11.2/ 7	13.6/ 10	10.0/ 7	14.4/ 8	10.5/ 7	17.1/ 8	33.7/ 17	20.4/ 10
-.35	4.1/ 3	13.8/ 7	10.9/ 6	13.0/ 9	16.2/ 10	5.4/ 4	23.4/ 12	22.7/ 13
-.25	3.4/ 2	10.4/ 7	8.4/ 6	3.2/ 2	6.6/ 5	13.1/ 7	16.5/ 12	12.3/ 7
-.15	7.6/ 5	14.5/ 10	12.3/ 9	9.9/ 8	13.2/ 8	12.7/ 8	8.6/ 6	11.5/ 7
-.05	8.1/ 6	15.9/ 11	14.5/ 10	9.4/ 6	11.5/ 4	12.5/ 5	14.5/ 9	16.7/ 11
+.05	26.5/ 19	34.7/ 26	32.0/ 22	27.5/ 16	15.9/ 9	11.2/ 7	16.7/ 10	9.5/ 5
+.15	25.9/ 19	38.1/ 28	45.6/ 30	16.0/ 12	11.8/ 8	26.0/ 19	18.9/ 12	13.0/ 8
+.25	23.8/ 17	53.2/ 38	53.3/ 38	47.4/ 29	23.8/ 16	17.5/ 11	22.9/ 15	13.7/ 9
+.35	30.5/ 23	58.4/ 43	51.6/ 37	41.7/ 31	34.6/ 24	23.9/ 17	17.9/ 13	19.6/ 14
+.45	49.1/ 39	92.6/ 70	65.3/ 49	63.5/ 47	34.5/ 25	16.1/ 12	49.5/ 33	21.5/ 16
+.55	41.6/ 32	124.9/ 99	80.9/ 63	80.3/ 62	32.7/ 26	26.2/ 20	52.0/ 39	29.2/ 20
+.65	54.7/ 44	106.1/ 87	91.1/ 71	57.7/ 46	25.3/ 20	33.9/ 27	59.1/ 47	29.6/ 22
+.75	56.3/ 46	114.4/ 93	95.8/ 79	77.5/ 63	46.4/ 37	36.1/ 29	47.3/ 38	16.3/ 12
+.85	42.1/ 35	119.9/100	61.6/ 51	61.2/ 51	36.0/ 30	21.7/ 18	66.8/ 55	40.8/ 34
+.95	39.9/ 24	102.2/ 63	67.8/ 44	52.7/ 31	13.1/ 10	35.6/ 20	75.1/ 49	47.5/ 30
TOTAL	497.7/366	1060.3/793	850.5/601	707.1/490	394.6/273	401.2/257	647.7/438	407.3/262

NUMBER WEIGHTED / NUMBER UNWEIGHTED

CENTER	2.051 GeV	2.085 GeV	2.106 GeV
-.95	33.5/ 14	23.8/ 9	9.2/ 5
-.85	9.7/ 5	6.3/ 4	4.3/ 3
-.75	4.9/ 3	1.4/ 1	4.9/ 3
-.65	21.4/ 11	3.5/ 2	7.1/ 4
-.55	21.0/ 9	8.8/ 3	12.5/ 7
-.45	13.4/ 7	28.4/ 14	21.7/ 12
-.35	15.1/ 8	15.4/ 9	20.5/ 11
-.25	17.5/ 9	19.4/ 11	13.7/ 8
-.15	12.5/ 6	15.0/ 9	29.8/ 18
-.05	16.5/ 9	7.1/ 4	12.9/ 8
+.05	11.5/ 7	20.8/ 11	7.5/ 4
+.15	15.3/ 9	14.2/ 10	27.5/ 15
+.25	17.6/ 13	20.9/ 14	21.6/ 13
+.35	15.3/ 11	19.2/ 15	26.2/ 19
+.45	12.2/ 8	17.8/ 13	18.2/ 14
+.55	13.1/ 10	13.6/ 11	16.4/ 12
+.65	20.0/ 15	14.6/ 10	8.9/ 7
+.75	26.0/ 21	10.2/ 8	12.2/ 10
+.85	20.8/ 17	30.3/ 25	17.0/ 14
+.95	37.4/ 24	44.1/ 30	80.4/ 49
TOTAL	354.8/216	334.8/213	372.7/236

Table III. Unnormalized angular distributions for $K^- p \rightarrow \overline{K}^0 n$ in twenty equal bins of $\cos\theta$.

NUMBER WEIGHTED / NUMBER UNWEIGHTED

CENTER	1.709 GeV	1.738 GeV	1.758 GeV	1.767 GeV	1.782 GeV	1.803 GeV	1.821 GeV	1.846 GeV
-.95	22.6/ 14	106.3/ 68	216.1/140	39.0/ 25	224.9/147	275.5/181	161.4/107	90.3/ 60
-.85	10.3/ 7	46.1/ 32	131.5/ 92	26.6/ 18	133.0/ 94	140.1/100	61.1/ 44	44.1/ 32
-.75	4.2/ 3	34.0/ 25	53.1/ 39	9.4/ 7	51.0/ 38	73.4/ 55	30.6/ 23	17.2/ 13
-.65	2.7/ 2	8.0/ 6	27.8/ 21	2.6/ 2	24.9/ 19	20.9/ 16	9.1/ 7	10.4/ 8
-.55	2.7/ 2	2.6/ 2	7.9/ 6	0. / 0	6.4/ 5	15.6/ 12	14.3/ 11	14.0/ 11
-.45	1.3/ 1	6.6/ 5	22.0/ 17	1.3/ 1	16.7/ 13	21.9/ 17	27.9/ 22	16.7/ 13
-.35	2.6/ 2	5.1/ 4	21.6/ 17	3.9/ 3	18.8/ 15	37.5/ 30	26.3/ 21	16.7/ 13
-.25	2.5/ 2	8.8/ 7	18.9/ 15	5.1/ 4	31.2/ 25	56.1/ 45	22.5/ 18	22.3/ 18
-.15	2.5/ 2	19.0/ 15	30.0/ 24	11.2/ 9	54.0/ 43	45.2/ 36	30.5/ 24	17.5/ 14
-.05	2.5/ 2	13.9/ 11	50.6/ 40	8.8/ 7	49.6/ 39	61.4/ 49	32.7/ 26	10.2/ 8
+.05	3.8/ 3	20.0/ 16	44.9/ 36	12.2/ 10	64.8/ 53	63.4/ 52	32.8/ 27	7.2/ 6
+.15	3.7/ 3	21.6/ 18	43.9/ 37	10.6/ 9	48.7/ 41	52.8/ 45	26.9/ 23	10.8/ 9
+.25	4.8/ 4	19.2/ 16	72.7/ 61	12.9/ 11	56.8/ 48	67.4/ 57	14.1/ 12	8.3/ 7
+.35	5.9/ 5	30.7/ 26	50.4/ 43	9.5/ 8	46.6/ 40	56.6/ 48	10.7/ 9	4.6/ 4
+.45	3.6/ 3	20.0/ 17	56.4/ 48	6.9/ 6	53.0/ 45	43.4/ 37	27.7/ 24	12.6/ 11
+.55	6.9/ 6	36.2/ 29	45.3/ 39	9.3/ 8	55.5/ 48	60.3/ 51	25.5/ 22	31.4/ 27
+.65	4.7/ 4	23.5/ 20	44.3/ 38	2.4/ 2	50.9/ 44	79.6/ 68	44.2/ 38	39.6/ 34
+.75	13.4/ 11	21.4/ 18	46.5/ 39	8.3/ 7	74.5/ 62	92.8/ 77	56.2/ 47	29.6/ 24
+.85	13.6/ 11	19.6/ 16	38.7/ 32	6.0/ 5	64.8/ 54	134.3/112	96.6/ 80	48.7/ 40
+.95	14.2/ 12	15.5/ 13	32.6/ 27	8.4/ 7	85.0/ 71	197.0/164	90.4/ 76	67.7/ 57
TOTAL	128.2/ 99	478.1/364	1055.1/811	193.3/149	1211.0/944	1595.2/1252	841.6/661	519.8/409

NUMBER WEIGHTED / NUMBER UNWEIGHTED

CENTER	1.865 GeV	1.887 GeV	1.919 GeV	1.937 GeV	1.953 GeV	1.970 GeV	2.001 GeV	2.022 GeV
-.95	97.0/ 61	257.0/150	142.2/ 90	81.8/ 53	52.0/ 33	40.5/ 26	78.9/ 51	32.4/ 21
-.85	32.6/ 23	102.3/ 73	53.0/ 40	37.3/ 27	16.7/ 12	16.7/ 12	16.4/ 12	9.3/ 7
-.75	21.5/ 16	45.4/ 34	34.7/ 26	19.7/ 15	7.9/ 6	9.2/ 7	10.5/ 8	2.6/ 2
-.65	22.2/ 17	32.4/ 25	25.8/ 20	14.0/ 11	7.8/ 6	6.5/ 5	20.5/ 16	7.4/ 6
-.55	20.0/ 16	32.9/ 26	28.8/ 23	17.5/ 14	10.0/ 8	7.6/ 6	24.1/ 19	16.2/ 13
-.45	27.7/ 22	46.2/ 37	32.5/ 26	26.3/ 21	15.1/ 12	8.9/ 7	27.5/ 22	15.9/ 13
-.35	27.7/ 22	72.2/ 58	37.7/ 30	18.7/ 15	9.9/ 8	12.4/ 10	25.0/ 20	9.9/ 8
-.25	29.7/ 24	80.9/ 65	22.0/ 18	18.9/ 15	9.8/ 8	5.9/ 5	6.5/ 5	12.2/ 10
-.15	21.9/ 18	53.2/ 43	20.6/ 17	6.3/ 5	6.2/ 5	1.2/ 1	6.1/ 5	7.0/ 6
-.05	18.4/ 15	32.9/ 27	20.7/ 17	3.5/ 3	1.3/ 1	8.3/ 7	7.4/ 6	9.9/ 8
+.05	9.8/ 8	30.3/ 25	7.3/ 6	3.8/ 3	0. / 0	1.3/ 1	12.4/ 10	12.5/ 10
+.15	12.0/ 10	16.0/ 13	1.2/ 1	7.6/ 6	4.9/ 4	9.9/ 8	21.1/ 17	10.0/ 8
+.25	7.1/ 6	15.6/ 13	9.7/ 8	9.7/ 8	12.4/ 10	8.7/ 7	28.8/ 22	33.3/ 27
+.35	10.6/ 9	24.5/ 20	23.4/ 19	13.4/ 11	14.6/ 12	15.3/ 12	40.2/ 33	27.8/ 23
+.45	18.2/ 15	34.9/ 29	23.6/ 20	33.8/ 28	12.0/ 10	15.7/ 13	39.3/ 32	26.0/ 21
+.55	38.0/ 32	47.4/ 40	36.3/ 30	34.2/ 28	14.2/ 12	13.4/ 11	36.5/ 30	20.3/ 17
+.65	40.7/ 33	80.0/ 67	42.7/ 36	37.4/ 31	17.7/ 15	14.0/ 12	40.2/ 34	21.9/ 19
+.75	57.9/ 50	78.3/ 68	29.8/ 26	26.1/ 23	21.0/ 17	14.5/ 12	47.1/ 40	21.8/ 19
+.85	52.9/ 45	91.6/ 79	40.8/ 35	20.0/ 17	22.7/ 19	17.5/ 15	58.6/ 50	49.5/ 43
+.95	47.4/ 41	90.1/ 77	38.3/ 33	28.3/ 23	23.0/ 20	18.5/ 16	58.0/ 49	52.5/ 44
TOTAL	613.6/483	1244.1/969	673.3/521	458.2/357	279.3/218	245.8/193	604.9/481	398.6/325

NUMBER WEIGHTED / NUMBER UNWEIGHTED

CENTER	2.051 GeV	2.085 GeV	2.106 GeV
-.95	36.4/ 24	25.8/ 17	18.4/ 12
-.85	2.7/ 2	5.4/ 4	5.4/ 4
-.75	6.4/ 5	2.6/ 2	3.8/ 3
-.65	8.9/ 7	15.0/ 12	16.3/ 13
-.55	18.9/ 15	10.0/ 8	12.6/ 10
-.45	6.3/ 5	16.2/ 13	13.7/ 11
-.35	8.8/ 7	5.2/ 4	7.5/ 6
-.25	4.7/ 4	2.5/ 2	15.0/ 12
-.15	6.1/ 5	4.0/ 3	7.4/ 6
-.05	3.8/ 3	16.2/ 12	16.0/ 13
+.05	7.8/ 6	15.2/ 12	18.7/ 15
+.15	12.7/ 10	21.1/ 17	13.8/ 11
+.25	14.9/ 12	22.4/ 18	21.7/ 17
+.35	19.0/ 16	25.1/ 20	22.0/ 17
+.45	18.9/ 15	10.0/ 8	15.9/ 13
+.55	14.5/ 12	11.2/ 9	17.7/ 15
+.65	15.6/ 13	18.2/ 15	27.6/ 23
+.75	22.8/ 19	28.2/ 23	31.3/ 26
+.85	27.8/ 23	54.0/ 45	48.3/ 41
+.95	50.7/ 42	59.9/ 50	91.0/ 76
TOTAL	307.6/245	368.0/294	423.9/344

Table IV. Sums of the lambda polarization cosine ($\sum_i \cos\chi_i$) in twenty equal bins of $\cos\theta$.

SUM OF POLAR COSINE / NUMBER UNWEIGHTED

CENTER	1.709 GeV	1.738 GeV	1.758 GeV	1.767 GeV	1.782 GeV	1.803 GeV	1.821 GeV	1.846 GeV
-.95	1.5/ 9	.5/ 62	1.2/100	-2.8/ 14	-2.2/ 69	-5.7/ 60	4.4/ 21	1.0/ 7
-.85	1.3/ 12	1.7/ 46	6.9/ 65	-.5/ 22	1.6/ 68	1.9/ 53	-4.1/ 16	.7/ 8
-.75	-.9/ 5	-5.1/ 31	4.7/ 69	1.3/ 14	3.4/ 59	-6.2/ 42	.6/ 14	1.7/ 12
-.65	1.6/ 9	1.0/ 39	5.0/ 49	-.3/ 10	4.1/ 43	7.1/ 54	1.1/ 18	.2/ 6
-.55	1.1/ 8	-3.9/ 27	-2.2/ 47	-.5/ 12	-1.6/ 39	4.3/ 40	1.6/ 10	-1.3/ 3
-.45	.4/ 7	.7/ 19	.6/ 39	.3/ 7	-1.8/ 37	-1.4/ 24	3.9/ 12	-.3/ 6
-.35	-.3/ 6	2.8/ 19	6.4/ 30	2.2/ 7	5.7/ 34	2.0/ 21	-2.3/ 6	-1.7/ 6
-.25	-1.5/ 7	2.4/ 18	4.7/ 42	-1.1/ 6	1.3/ 34	-6.6/ 31	-2.3/ 8	-.5/ 5
-.15	-1.2/ 5	-.3/ 13	3.4/ 32	.6/ 5	.4/ 33	1.9/ 31	1.7/ 10	.2/ 3
-.05	-.8/ 2	-2.1/ 14	8.3/ 32	.3/ 8	8.6/ 36	3.4/ 23	.2/ 8	.8/ 2
+.05	.2/ 1	.1/ 9	4.1/ 21	1.2/ 8	10.6/ 37	3.4/ 24	-.1/ 11	-1.0/ 8
+.15	.1/ 1	2.1/ 12	2.8/ 18	-1.1/ 4	7.0/ 31	5.9/ 27	4.0/ 12	-.8/ 7
+.25	.6/ 3	.2/ 1	-.3/ 20	.9/ 5	6.1/ 39	3.8/ 33	2.9/ 17	3.5/ 9
+.35	-.5/ 1	.3/ 3	5.7/ 18	-.1/ 4	1.8/ 36	6.4/ 44	3.7/ 24	.3/ 7
+.45	-1.8/ 2	.6/ 10	-1.3/ 13	1.2/ 3	-1.1/ 44	-2.0/ 41	.4/ 17	4.4/ 17
+.55	-.1/ 1	-1.8/ 9	-6.1/ 34	.2/ 4	-6.5/ 40	-4.2/ 67	-4.7/ 22	-1.1/ 15
+.65	.3/ 9	-4.7/ 21	-9.4/ 43	-.9/ 6	-8.4/ 51	-3.0/ 61	-1.5/ 35	3.6/ 27
+.75	-1.8/ 9	-2.3/ 29	-12.9/ 51	-2.0/ 14	-11.6/ 54	-12.5/ 55	-5.0/ 33	-7.0/ 21
+.85	-1.7/ 14	-11.8/ 45	-17.2/ 87	-.8/ 12	-10.3/ 87	-16.0/ 78	-5.2/ 33	-2.5/ 31
+.95	1.3/ 12	1.6/ 45	-13.5/ 91	-.4/ 21	-15.2/ 99	-16.5/ 90	-1.0/ 25	-5.5/ 17
TOTAL	/123	/472	/901	/186	/970	/899	/352	/217

SUM OF POLAR COSINE / NUMBER UNWEIGHTED

CENTER	1.865 GeV	1.887 GeV	1.919 GeV	1.937 GeV	1.953 GeV	1.970 GeV	2.001 GeV	2.022 GeV
-.95	.5/ 6	1.4/ 27	4.5/ 20	.2/ 26	.1/ 11	-1.8/ 11	-5.0/ 20	.6/ 10
-.85	-.8/ 7	-1.5/ 24	-.9/ 16	-.1/ 11	.0/ 3	.5/ 6	-3.4/ 9	-.9/ 8
-.75	3.2/ 15	1.9/ 23	.4/ 17	-.5/ 4	-2.6/ 6	-.4/ 5	-1.7/ 10	-1.2/ 6
-.65	.4/ 9	-.5/ 15	-.2/ 17	-6.4/ 17	-4.0/ 8	-3.1/ 11	-2.3/ 8	1.7/ 10
-.55	-2.6/ 8	2.1/ 12	-2.6/ 9	-.8/ 11	-2.8/ 6	-.9/ 12	-2.1/ 24	-1.3/ 10
-.45	2.0/ 7	.0/ 10	-.6/ 7	-1.1/ 8	-1.3/ 7	1.5/ 8	-2.0/ 17	2.8/ 10
-.35	.3/ 3	.4/ 7	-.4/ 6	1.0/ 9	-1.6/ 10	.2/ 4	1.2/ 12	2.1/ 13
-.25	1.0/ 2	-1.7/ 7	1.4/ 6	-.6/ 2	-1.3/ 5	.3/ 7	.8/ 12	1.7/ 7
-.15	.8/ 5	-.2/ 10	3.4/ 9	1.6/ 8	-.8/ 8	-.6/ 8	.7/ 6	2.3/ 7
-.05	-.0/ 6	1.1/ 11	-.4/ 10	-1.3/ 6	.9/ 4	-.4/ 5	-.2/ 9	1.4/ 11
+.05	8.2/ 19	.8/ 26	-1.2/ 22	-.7/ 16	2.8/ 9	.5/ 7	-.2/ 10	1.4/ 5
+.15	3.0/ 19	2.4/ 28	3.2/ 30	1.8/ 12	1.2/ 8	4.7/ 19	-1.9/ 12	-2.0/ 8
+.25	5.1/ 17	2.1/ 38	-2.0/ 38	-.3/ 29	.1/ 16	-3.9/ 11	-4.4/ 15	-1.9/ 9
+.35	3.2/ 23	14.2/ 43	-7.1/ 37	1.6/ 31	-.6/ 24	.6/ 17	-2.0/ 13	-2.9/ 14
+.45	7.0/ 39	2.8/ 70	11.4/ 49	.8/ 47	2.0/ 25	-4.1/ 12	-2.7/ 33	-5.1/ 16
+.55	2.3/ 32	5.6/ 99	.3/ 63	5.5/ 62	-.6/ 26	4.8/ 20	-10.2/ 39	-4.5/ 20
+.65	-4.8/ 44	-4.8/ 87	5.1/ 71	8.1/ 46	6.3/ 20	-3.1/ 27	-6.8/ 47	-1.2/ 22
+.75	-.5/ 46	-4.0/ 93	-6.7/ 79	6.9/ 63	-2.9/ 37	-2.7/ 29	-5.7/ 38	1.3/ 12
+.85	-4.4/ 35	-2.4/100	-10.8/ 51	-4.3/ 51	.0/ 30	-5.6/ 18	4.3/ 55	8.8/ 34
+.95	-1.5/ 24	-17.7/ 63	-3.9/ 44	-.6/ 31	-2.9/ 10	-1.3/ 20	5.1/ 49	-1.1/ 30
TOTAL	/366	/793	/601	/490	/273	/257	/438	/262

SUM OF POLAR COSINE / NUMBER UNWEIGHTED

CENTER	2.051 GeV	2.085 GeV	2.106 GeV
-.95	-1.3/ 14	-.3/ 9	1.2/ 5
-.85	-.2/ 5	.2/ 4	-.1/ 3
-.75	-.2/ 3	.7/ 1	-1.1/ 3
-.65	-.7/ 11	-.6/ 2	-1.3/ 4
-.55	-1.6/ 9	-1.7/ 3	-.6/ 7
-.45	3.5/ 7	5.6/ 14	-3.2/ 12
-.35	-.5/ 8	.4/ 9	.4/ 11
-.25	2.5/ 9	2.2/ 11	-.4/ 8
-.15	.9/ 6	1.0/ 9	5.2/ 18
-.05	.6/ 9	.2/ 4	1.1/ 8
+.05	1.6/ 7	1.7/ 11	.9/ 4
+.15	1.2/ 9	-.8/ 10	.0/ 15
+.25	-4.0/ 13	-3.0/ 14	-1.3/ 13
+.35	-.3/ 11	-1.0/ 15	-5.7/ 19
+.45	-2.1/ 8	-1.9/ 13	-3.8/ 14
+.55	-1.7/ 10	-1.6/ 11	-1.0/ 12
+.65	-1.8/ 15	-1.2/ 10	-1.9/ 7
+.75	.4/ 21	-.0/ 8	.6/ 10
+.85	1.1/ 17	1.7/ 25	3.0/ 14
+.95	4.8/ 24	5.4/ 30	7.1/ 49
TOTAL	/216	/213	/236

Table V. Legendre expansion coefficients for $\Lambda\pi^0$ angular distributions.

$E_{c.m.}$	10^{+3} A_0	10^{+3} A_1	10^{+3} A_2	10^{+3} A_3	10^{+3} A_4	10^{+3} A_5	10^{+3} A_6	10^{+3} A_7
1.709	114 ± 12	9 ± 24	158 ± 31	111 ± 37	25 ± 42	-42 ± 48	19 ± 46	0 ± 0
1.738	145 ± 9	-42 ± 16	235 ± 22	67 ± 25	105 ± 28	-9 ± 26	13 ± 27	0 ± 0
1.758	156 ± 10	-33 ± 12	210 ± 19	65 ± 19	82 ± 22	1 ± 21	4 ± 22	0 ± 0
1.767	196 ± 18	-52 ± 33	250 ± 43	88 ± 50	82 ± 58	92 ± 55	-72 ± 65	0 ± 0
1.782	175 ± 11	13 ± 12	172 ± 18	66 ± 20	87 ± 22	72 ± 22	36 ± 24	0 ± 0
1.803	153 ± 9	23 ± 11	155 ± 16	8 ± 18	39 ± 20	42 ± 20	33 ± 22	0 ± 0
1.821	151 ± 11	42 ± 17	116 ± 21	-20 ± 25	-36 ± 30	4 ± 32	-13 ± 35	0 ± 0
1.846	121 ± 11	82 ± 18	107 ± 21	-6 ± 25	-56 ± 29	-0 ± 31	-55 ± 39	0 ± 0
1.865	123 ± 9	117 ± 15	60 ± 16	-71 ± 20	-80 ± 24	17 ± 26	-5 ± 29	-11 ± 30
1.887	113 ± 8	120 ± 12	85 ± 12	-58 ± 15	-57 ± 15	-6 ± 17	3 ± 17	10 ± 18
1.919	104 ± 9	83 ± 11	62 ± 12	-85 ± 15	-43 ± 17	8 ± 18	6 ± 18	8 ± 20
1.937	109 ± 7	84 ± 12	81 ± 14	-87 ± 18	-41 ± 20	-43 ± 22	66 ± 22	-37 ± 23
1.953	105 ± 9	65 ± 13	26 ± 16	-80 ± 20	-44 ± 22	-68 ± 26	15 ± 28	-49 ± 30
1.970	119 ± 10	46 ± 16	48 ± 20	-17 ± 24	-24 ± 29	5 ± 31	29 ± 33	-41 ± 39
2.001	120 ± 8	81 ± 13	104 ± 16	19 ± 19	-16 ± 22	-38 ± 24	70 ± 25	-21 ± 28
2.022	114 ± 10	51 ± 15	73 ± 20	40 ± 24	27 ± 26	10 ± 29	86 ± 31	11 ± 35
2.051	116 ± 11	24 ± 16	57 ± 23	14 ± 29	62 ± 33	-53 ± 35	69 ± 34	-62 ± 40
2.085	121 ± 11	60 ± 18	58 ± 24	33 ± 31	147 ± 33	3 ± 35	123 ± 36	-25 ± 39
2.106	95 ± 8	69 ± 13	40 ± 17	91 ± 23	124 ± 23	80 ± 31	147 ± 33	19 ± 41

Table VI. Associated Legendre expansion coefficients for $\Lambda\pi^0$ polarization distributions.

$E_{c.m.}$	10^{+3} B_0	10^{+3} B_1	10^{+3} B_2	10^{+3} B_3	10^{+3} B_4	10^{+3} B_5	10^{+3} B_6	10^{+3} B_7
1.709	0 ± 0	-17 ± 18	-29 ± 18	9 ± 17	-16 ± 16	4 ± 13	9 ± 17	0 ± 0
1.738	0 ± 0	-25 ± 13	-27 ± 14	-40 ± 14	-18 ± 13	-15 ± 9	-7 ± 9	0 ± 0
1.758	0 ± 0	14 ± 13	-66 ± 13	-41 ± 12	-36 ± 10	-5 ± 8	-11 ± 8	0 ± 0
1.767	0 ± 0	1 ± 23	-7 ± 23	-52 ± 22	10 ± 20	-16 ± 16	8 ± 15	0 ± 0
1.782	0 ± 0	20 ± 15	-41 ± 14	-48 ± 12	-24 ± 11	7 ± 9	8 ± 9	0 ± 0
1.803	0 ± 0	-7 ± 13	-28 ± 12	-50 ± 11	-28 ± 10	-17 ± 8	9 ± 8	0 ± 0
1.821	0 ± 0	8 ± 17	-36 ± 16	-32 ± 15	-23 ± 13	-7 ± 10	15 ± 10	0 ± 0
1.846	0 ± 0	-4 ± 16	-22 ± 16	-26 ± 14	-57 ± 13	-20 ± 11	-12 ± 9	0 ± 0
1.865	0 ± 0	50 ± 15	-1 ± 14	-29 ± 12	-30 ± 10	-2 ± 10	11 ± 8	9 ± 7
1.887	0 ± 0	19 ± 11	-3 ± 10	-24 ± 8	-34 ± 7	-22 ± 7	-7 ± 5	-0 ± 4
1.919	0 ± 0	1 ± 11	-11 ± 10	-12 ± 8	-23 ± 7	-6 ± 7	-13 ± 6	2 ± 5
1.937	0 ± 0	13 ± 12	31 ± 11	2 ± 9	-11 ± 9	-7 ± 8	-17 ± 6	1 ± 6
1.953	0 ± 0	-6 ± 13	30 ± 11	-20 ± 9	-17 ± 9	-1 ± 7	-10 ± 6	-6 ± 7
1.970	0 ± 0	-24 ± 14	-11 ± 12	-31 ± 11	-2 ± 9	-8 ± 11	-3 ± 10	-3 ± 9
2.001	0 ± 0	-52 ± 12	-12 ± 12	-14 ± 10	31 ± 9	19 ± 9	13 ± 7	5 ± 6
2.022	0 ± 0	3 ± 14	-19 ± 11	9 ± 11	49 ± 11	23 ± 11	-1 ± 9	-4 ± 8
2.051	0 ± 0	10 ± 12	-10 ± 10	-1 ± 9	26 ± 9	17 ± 11	-2 ± 9	3 ± 9
2.085	0 ± 0	15 ± 18	-21 ± 13	11 ± 13	32 ± 12	26 ± 13	-5 ± 11	14 ± 11
2.106	0 ± 0	-17 ± 11	-8 ± 8	2 ± 7	13 ± 7	22 ± 7	-8 ± 6	-10 ± 6

Table VII. Legendre expansion coefficients for $\overline{K}^0 n$ angular distributions.

$E_{c.m.}$	10^{+3} A_0	10^{+3} A_1	10^{+3} A_2	10^{+3} A_3	10^{+3} A_4	10^{+3} A_5	10^{+3} A_6	10^{+3} A_7
1.709	172 ± 20	29 ± 40	279 ± 54	-119 ± 61	170 ± 68	-137 ± 86	24 ± 100	-127 ± 118
1.738	209 ± 14	-98 ± 23	234 ± 33	-359 ± 39	207 ± 41	-107 ± 44	30 ± 45	31 ± 51
1.758	257 ± 17	-139 ± 20	261 ± 29	-419 ± 38	277 ± 36	-109 ± 36	27 ± 36	-14 ± 38
1.767	294 ± 29	-165 ± 49	256 ± 73	-430 ± 87	464 ± 92	-14 ±130	-47 ± 124	166 ± 200
1.782	304 ± 19	-77 ± 21	335 ± 34	-340 ± 38	349 ± 41	-116 ± 41	-29 ± 40	29 ± 44
1.803	382 ± 22	12 ± 24	540 ± 42	-212 ± 39	522 ± 48	-144 ± 47	30 ± 44	30 ± 49
1.821	514 ± 34	-1 ± 44	797 ± 74	-243 ± 70	665 ± 82	-589 ± 91	15 ± 83	-134 ± 91
1.846	415 ± 30	11 ± 46	687 ± 71	-102 ± 73	414 ± 82	-357 ± 90	206 ± 81	126 ± 97
1.865	292 ± 21	2 ± 28	343 ± 41	-83 ± 43	102 ± 50	-387 ± 60	74 ± 54	-29 ± 61
1.887	263 ± 19	-84 ± 19	334 ± 32	-139 ± 30	226 ± 34	-343 ± 42	111 ± 35	53 ± 38
1.919	164 ± 14	-88 ± 17	223 ± 26	-125 ± 26	92 ± 28	-182 ± 33	152 ± 31	17 ± 33
1.937	139 ± 10	-37 ± 16	171 ± 21	-132 ± 25	34 ± 28	-115 ± 31	161 ± 31	32 ± 33
1.953	148 ± 13	-9 ± 22	209 ± 30	-118 ± 36	89 ± 38	-156 ± 44	168 ± 43	-89 ± 53
1.970	142 ± 13	-4 ± 22	164 ± 29	-133 ± 35	85 ± 38	-76 ± 44	126 ± 45	-63 ± 47
2.001	214 ± 15	85 ± 21	219 ± 28	-119 ± 32	72 ± 35	-126 ± 41	222 ± 42	-201 ± 44
2.022	214 ± 17	149 ± 25	192 ± 33	-10 ± 38	165 ± 41	-22 ± 48	217 ± 51	-107 ± 55
2.051	189 ± 17	119 ± 27	220 ± 37	-8 ± 44	171 ± 49	-12 ± 53	218 ± 52	-150 ± 57
2.085	239 ± 20	218 ± 31	246 ± 41	80 ± 46	204 ± 53	7 ± 56	15 ± 60	-375 ± 65
2.106	199 ± 15	214 ± 25	211 ± 32	157 ± 37	174 ± 42	71 ± 44	96 ± 44	-101 ± 48

FIGURE CAPTIONS

Fig. 1. Distribution of the Incident K^- Momenta for Final $\Lambda\pi^0$ Events.

Fig. 2. Missing Mass Squared to the Lambda--All Events ($K^-p \rightarrow \Lambda + MM$).

Fig. 3. Missing Mass Squared to the K-Zero--All Events ($K^-p \rightarrow \bar{K}^0 + MM$).

Fig. 4. Combined Angular Distributions Illustrating the Effects of Weighting. The cross-hatched histograms are unweighted events; the plain histograms are the final events resulting from application of the weights discussed in Section D. (a) $\Lambda\pi^0$ events; (b) $\bar{K}^0n$ events.

Fig. 5. Angular Distributions for the Reaction $K^-p \rightarrow \Lambda\pi^0$ (dN/d cos θ). The dashed line is the Legendre polynomial fit to the data. (a) 1709-1846 MeV; (b) 1865-2106 MeV.

Fig. 6. Polarization Distributions for the Reaction $K^-p \rightarrow \Lambda\pi^0$ (P dN/d cos θ). The dashed line is the Associated Legendre Polynomial fit to the data. (a) 1709-1846 MeV; (b) 1865-2106 MeV.

Fig. 7. Angular Distributions for the Reaction $K^-p \rightarrow \bar{K}^0n$ (dN/d cos θ). The dashed line is the seventh order Legendre Polynomial fit to the data. (a) 1709-1846 MeV; (b) 1865-2106 MeV.

Fig. 8. Legendre Expansion Coefficients for $\Lambda\pi^0$ Angular Distributions as a Function of Energy. Coefficients from References 1c, 2c, and 2f are shown for comparison.

Fig. 9. Associated Legendre Expansion Coefficients for the Lambda Polarization Distributions as a Function of Energy. Coefficients from References 1c, 2c, and 2f are shown for comparison.

Fig. 10. Legendre Expansion Coefficients for $\bar{K}^{o}n$ Angular Distributions as a Function of Energy. Representative A_o coefficients obtained from cross section data in References 1a, 1b, 1d, and 1e are shown for comparison.

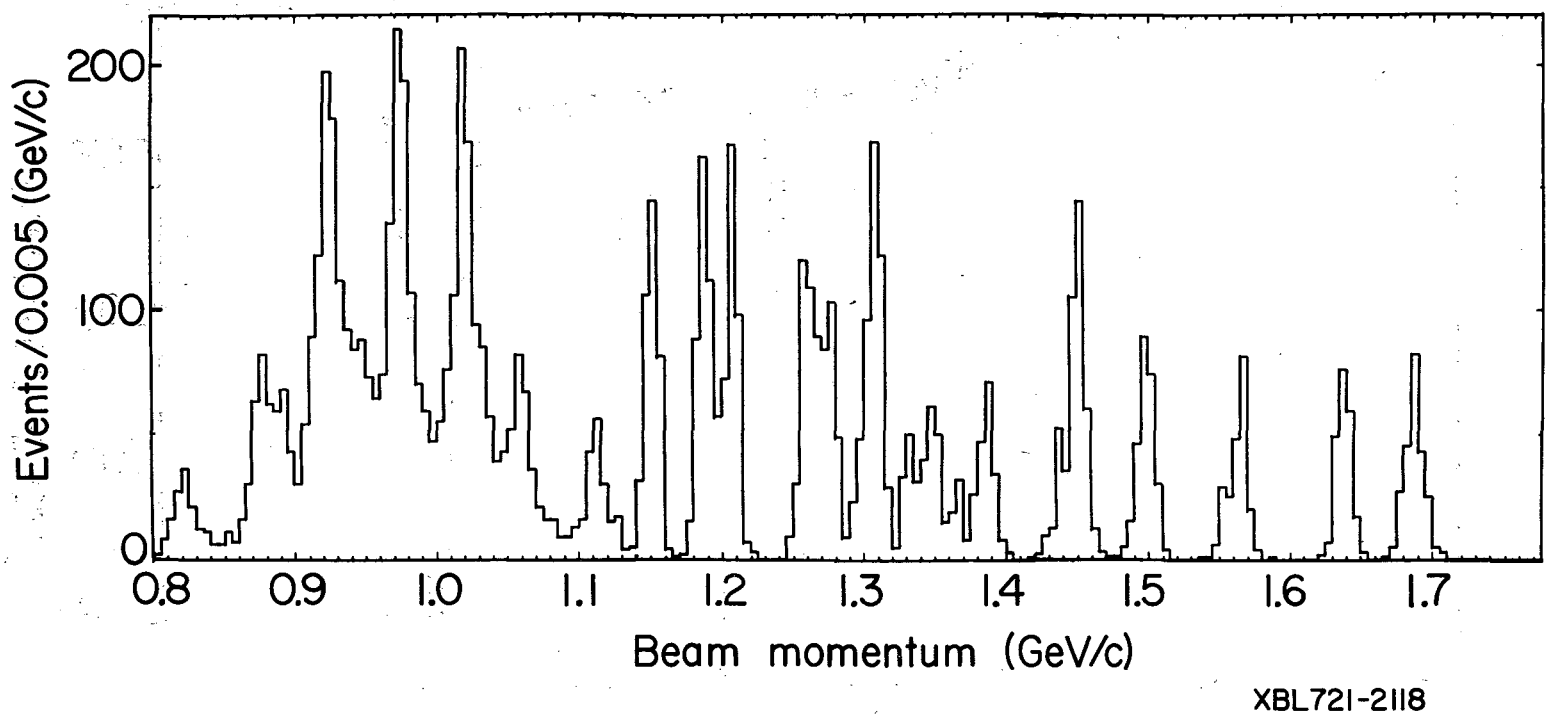
Events/0.005 (GeV/c)
200
100
0
0.8
0.9
1.0
1.1
1.2
1.3
1.4
1.5
1.6
1.7
Beam momentum (GeV/c)
XBL721-2118

Fig. 1

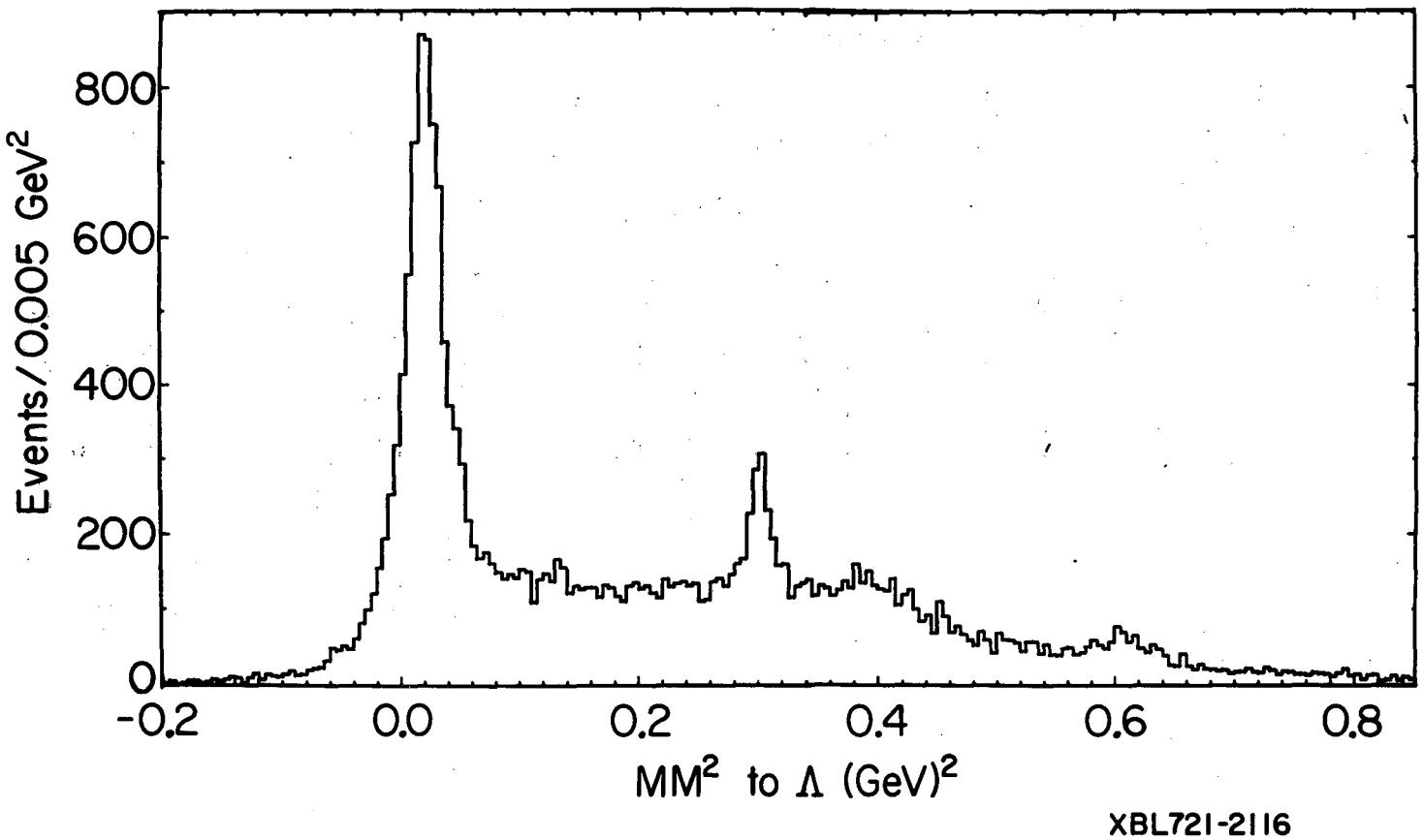
Events/0.005 GeV^2
800
600
400
200
0
-0.2
0.0
0.2
0.4
0.6
0.8
MM^2 to Λ (GeV)^2
XBL721-2116

Fig. 2

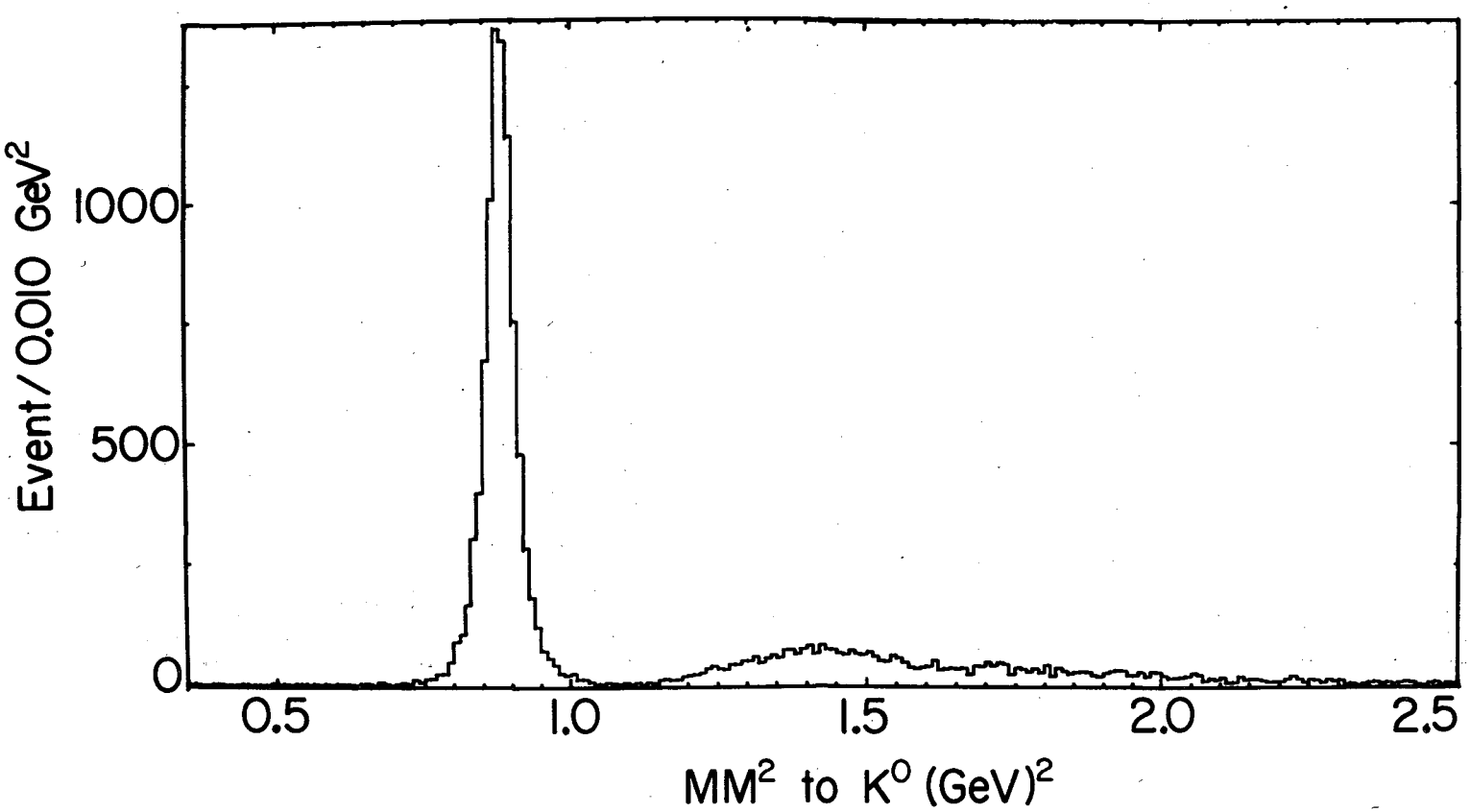

XBL721-2117

Fig. 3

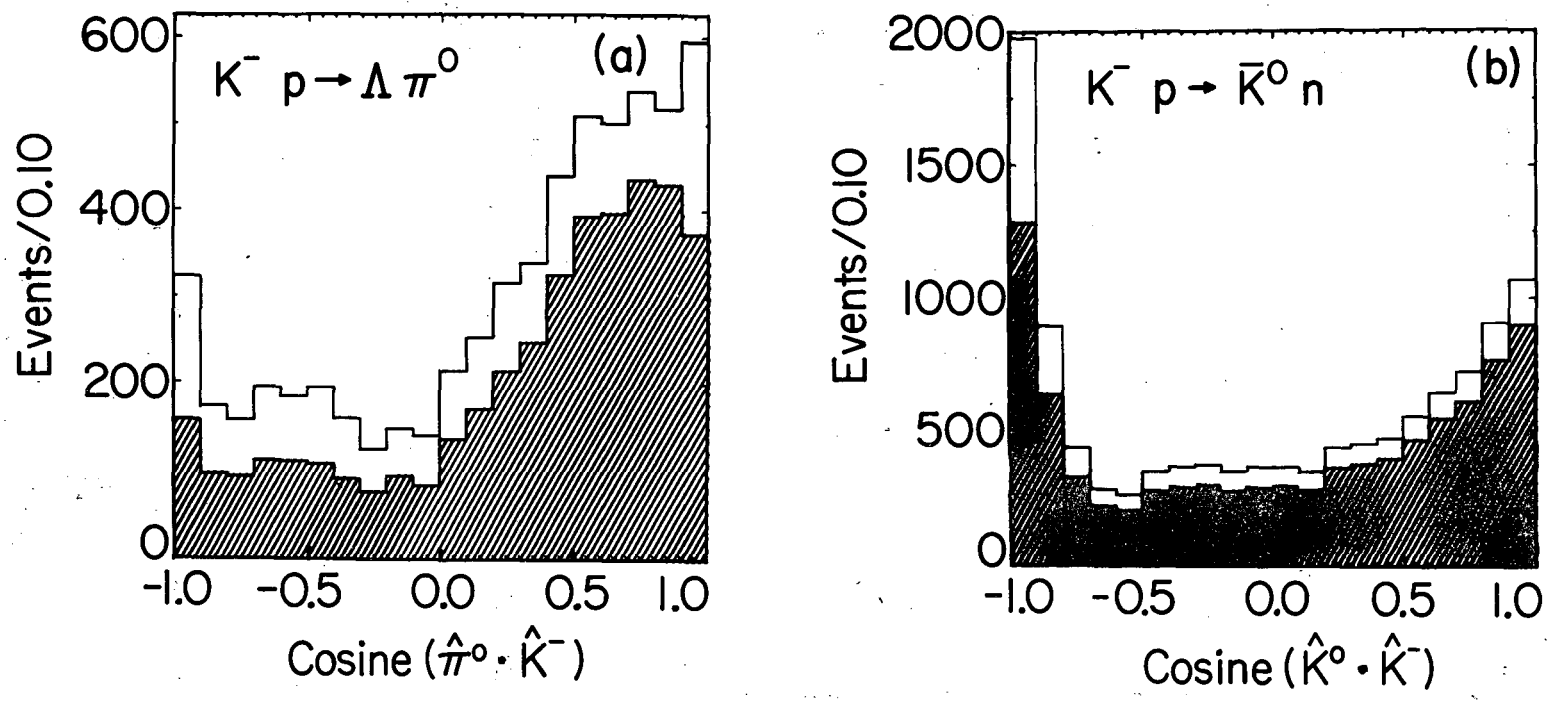

XBL721-2119

Fig. 4

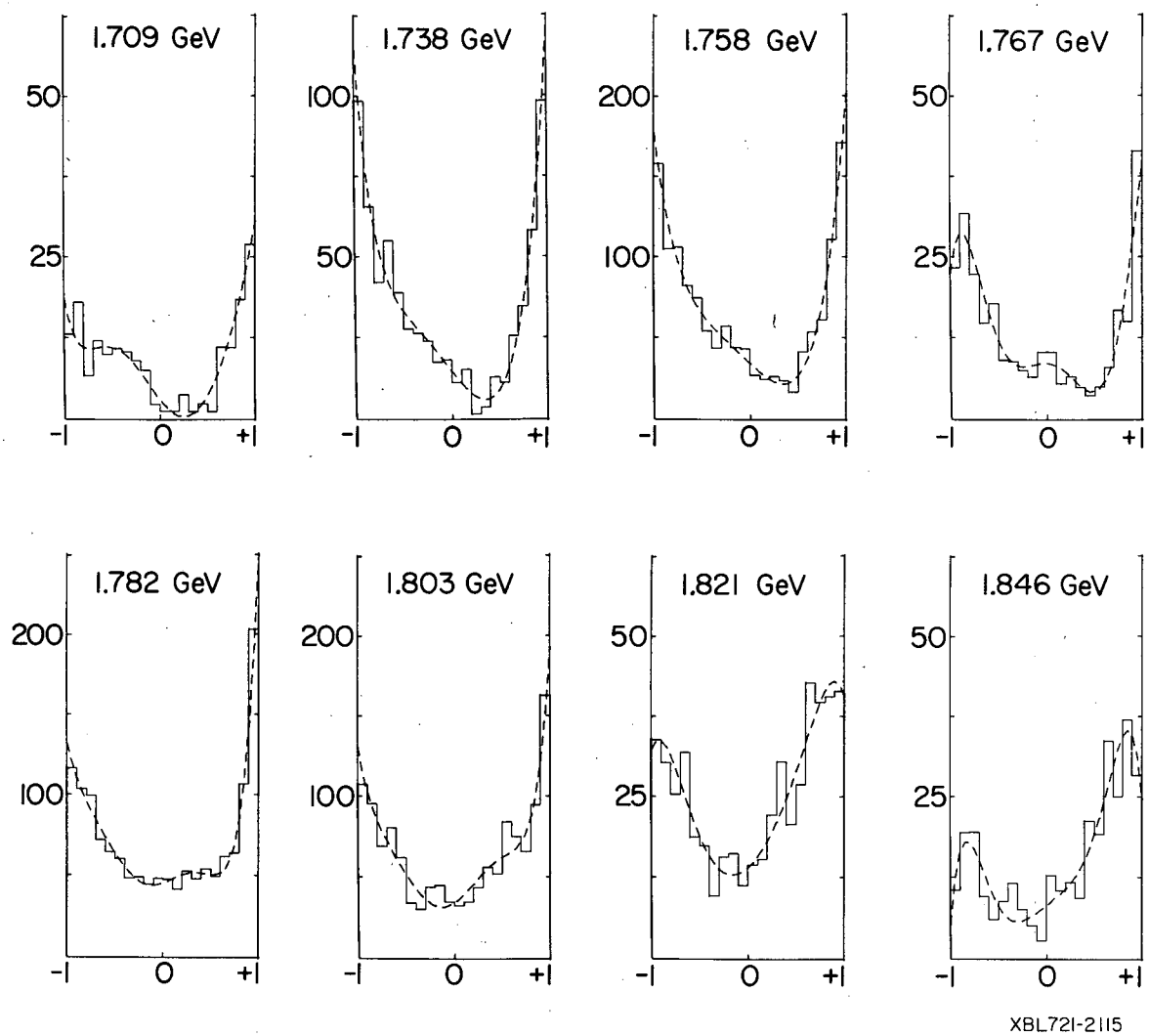
1.709 GeV
1.738 GeV
1.758 GeV
1.767 GeV
1.782 GeV
1.803 GeV
1.821 GeV
1.846 GeV
50
25
100
200
-1
0
+1
XBL721-2115

Fig. 5a

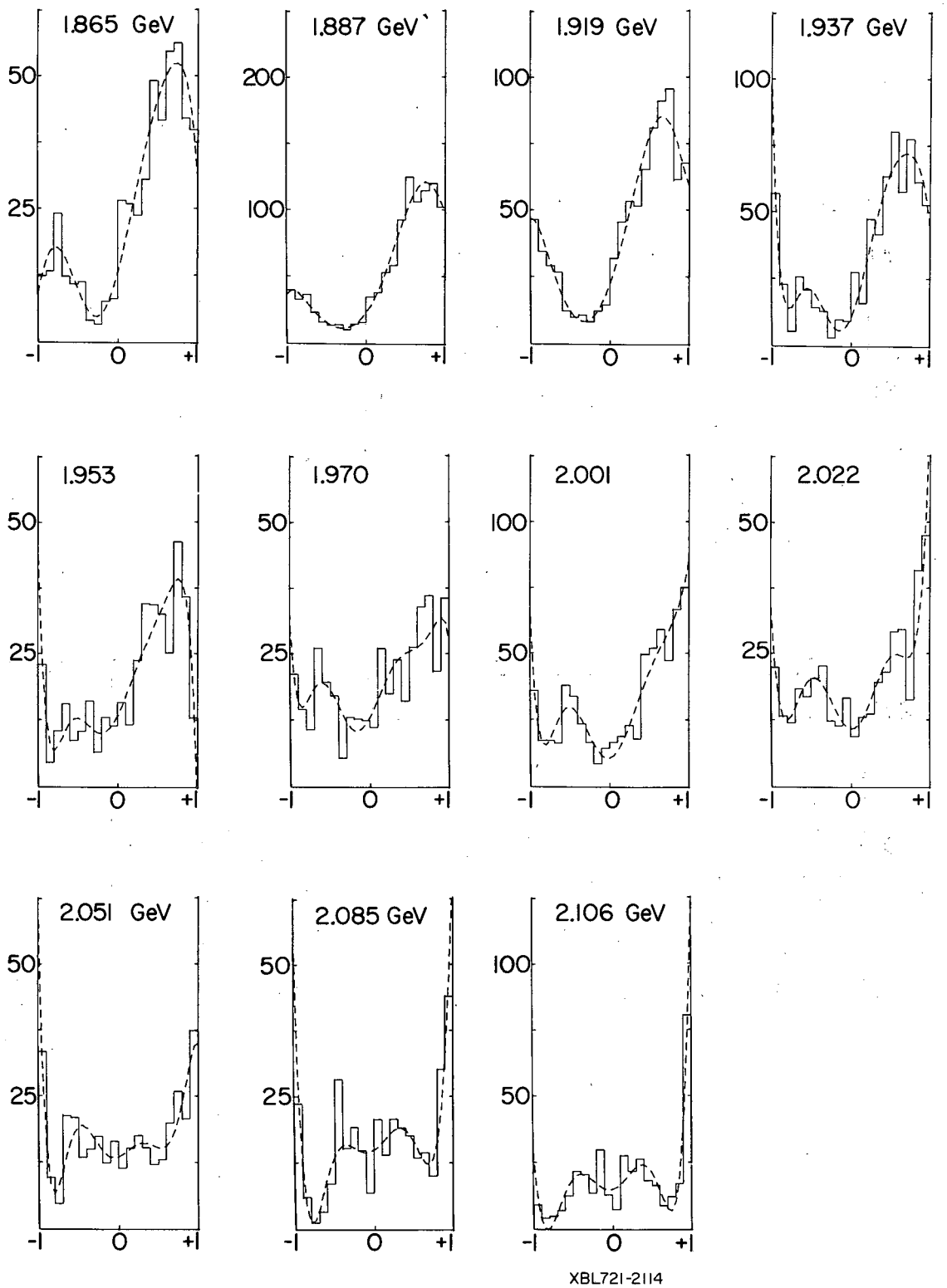
1.865 GeV
1.887 GeV
1.919 GeV
1.937 GeV
1.953
1.970
2.001
2.022
2.051 GeV
2.085 GeV
2.106 GeV
XBL721-2114

Fig. 5b

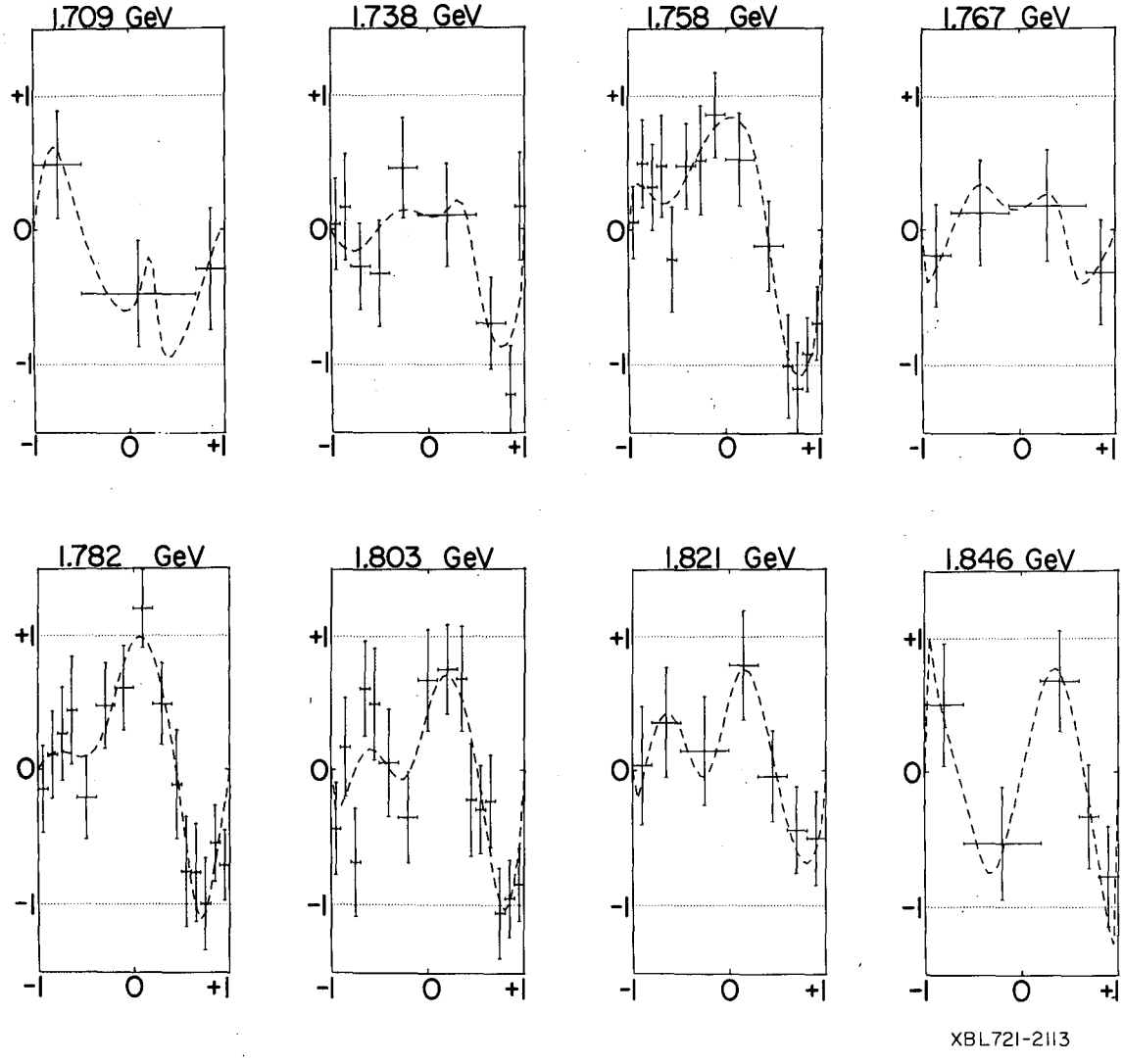
1.709 GeV
1.738 GeV
1.758 GeV
1.767 GeV
1.782 GeV
1.803 GeV
1.821 GeV
1.846 GeV
+1
0
-1
-1
0
+1
XBL721-2113

Fig. 6a

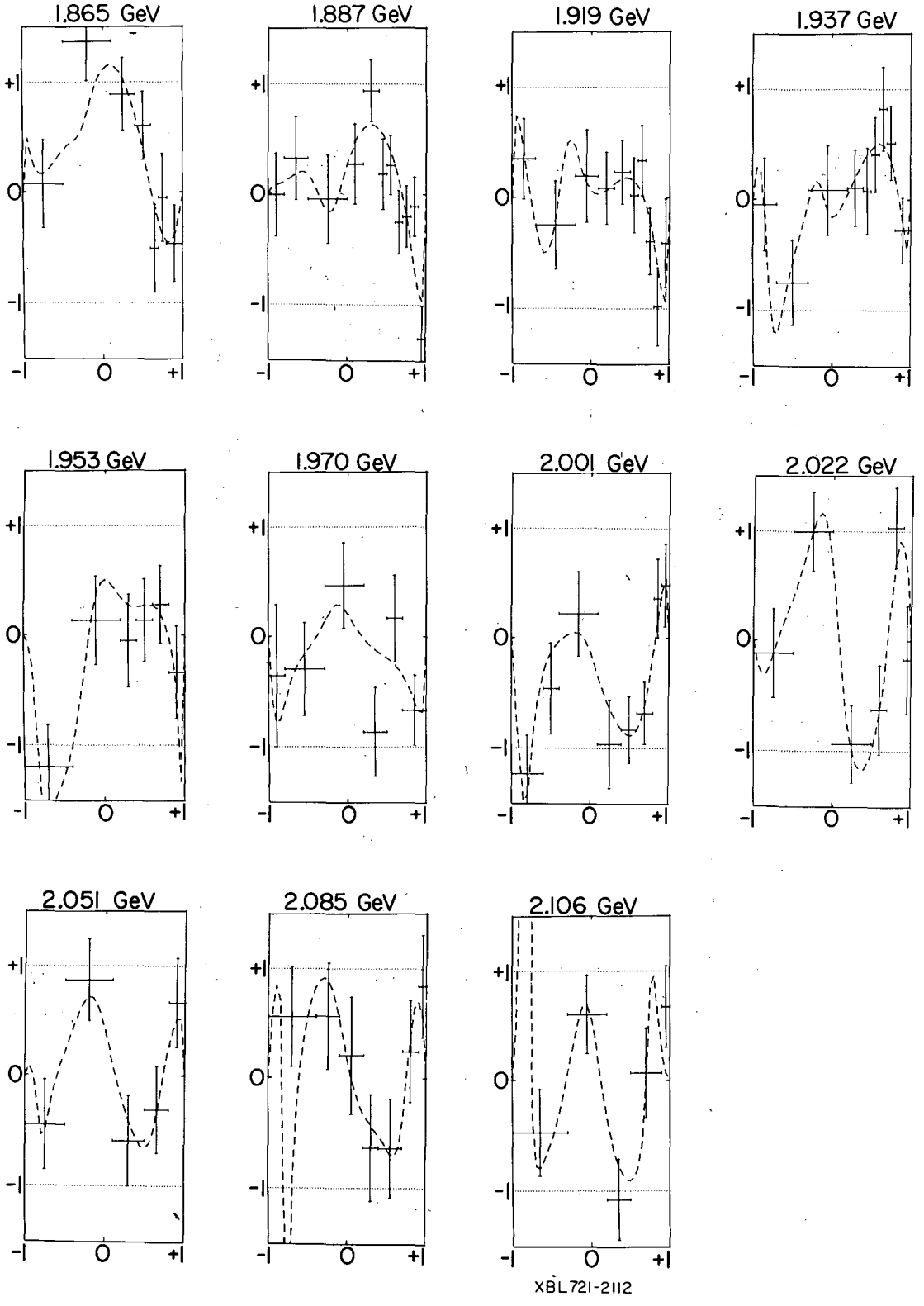
1.865 GeV
1.887 GeV
1.919 GeV
1.937 GeV
1.953 GeV
1.970 GeV
2.001 GeV
2.022 GeV
2.051 GeV
2.085 GeV
2.106 GeV
+1
0
-1
XBL721-2112

Fig. 6b

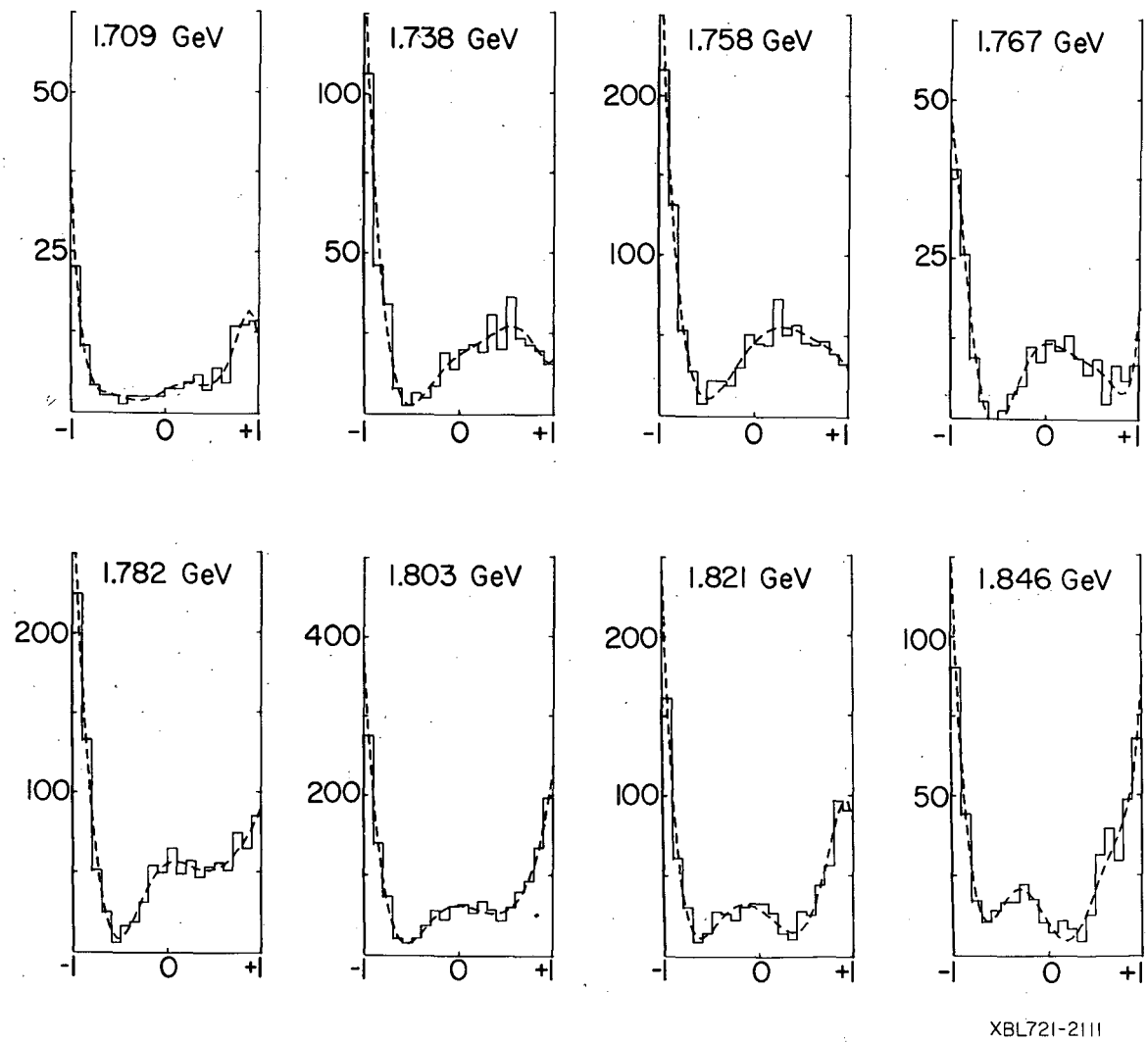
1.709 GeV
1.738 GeV
1.758 GeV
1.767 GeV
1.782 GeV
1.803 GeV
1.821 GeV
1.846 GeV
XBL721-2111

Fig. 7a

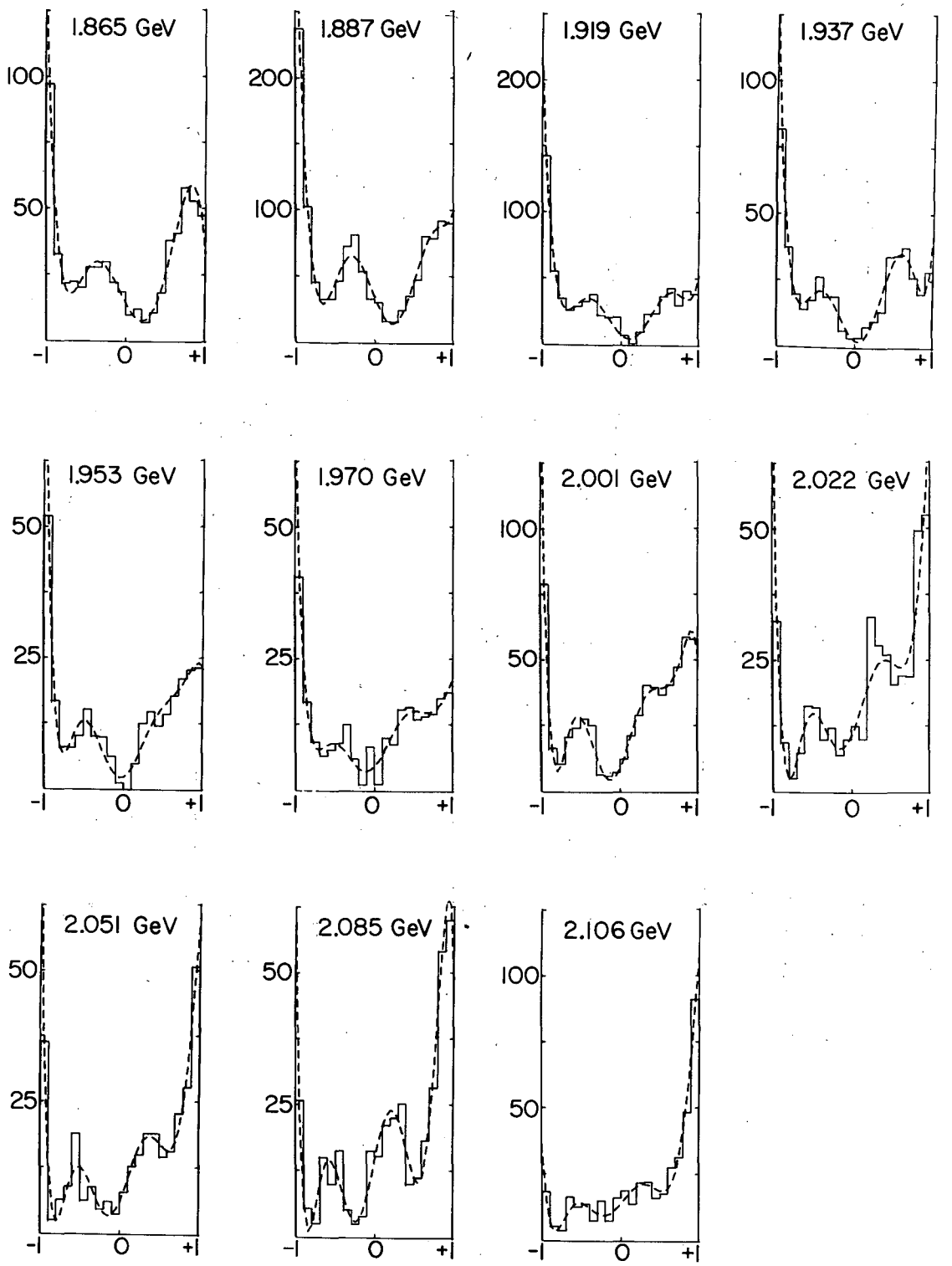

XBL721-2110

Fig. 7b

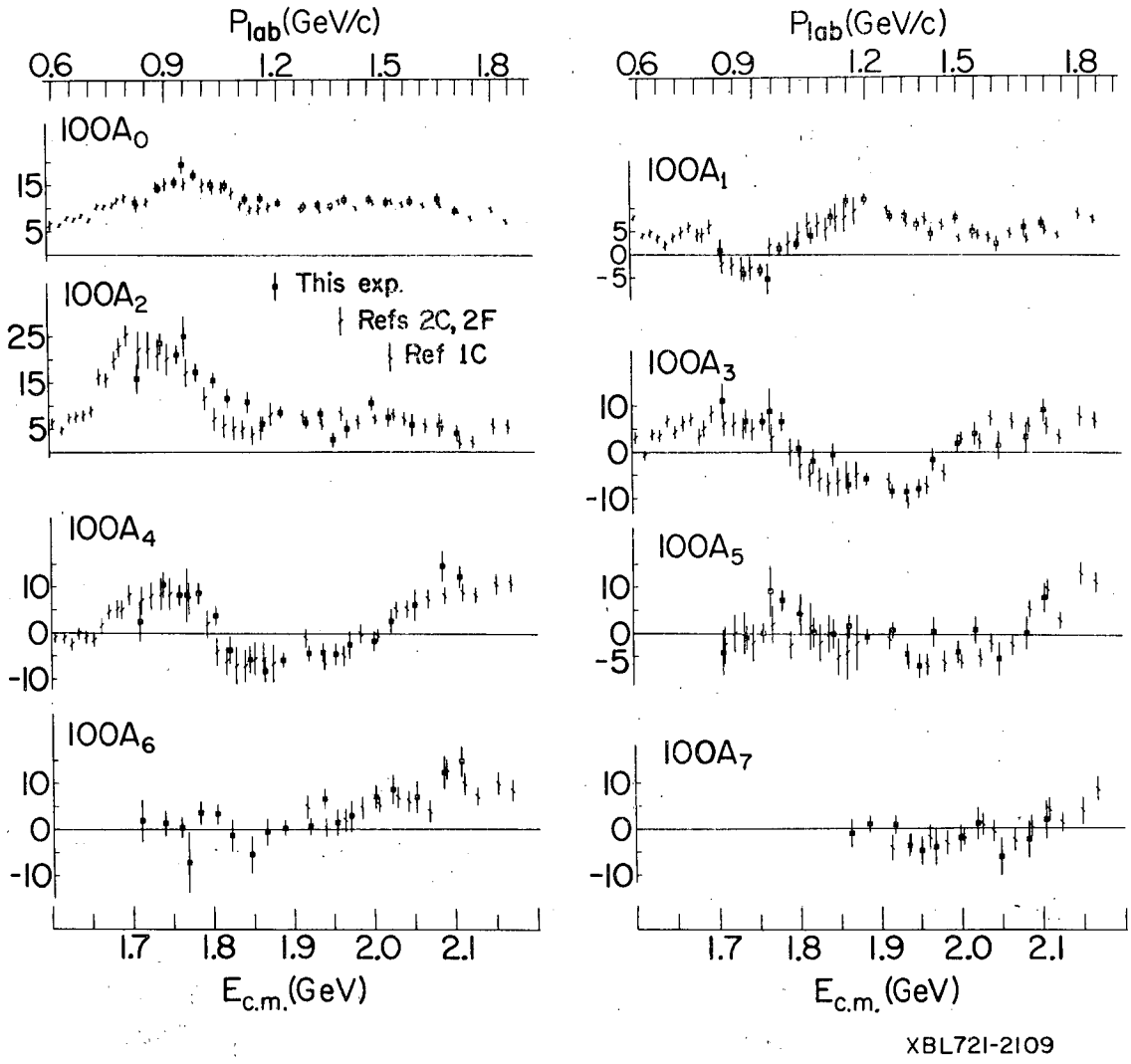
P_{lab}(GeV/c)
0.6
0.9
1.2
1.5
1.8
$100A_0$
$100A_1$
$100A_2$
$100A_3$
$100A_4$
$100A_5$
$100A_6$
$100A_7$
This exp.
Refs 2C, 2F
Ref 1C
1.7
1.8
1.9
2.0
2.1
$E_{c.m.}$(GeV)
XBL721-2109

Fig. 8

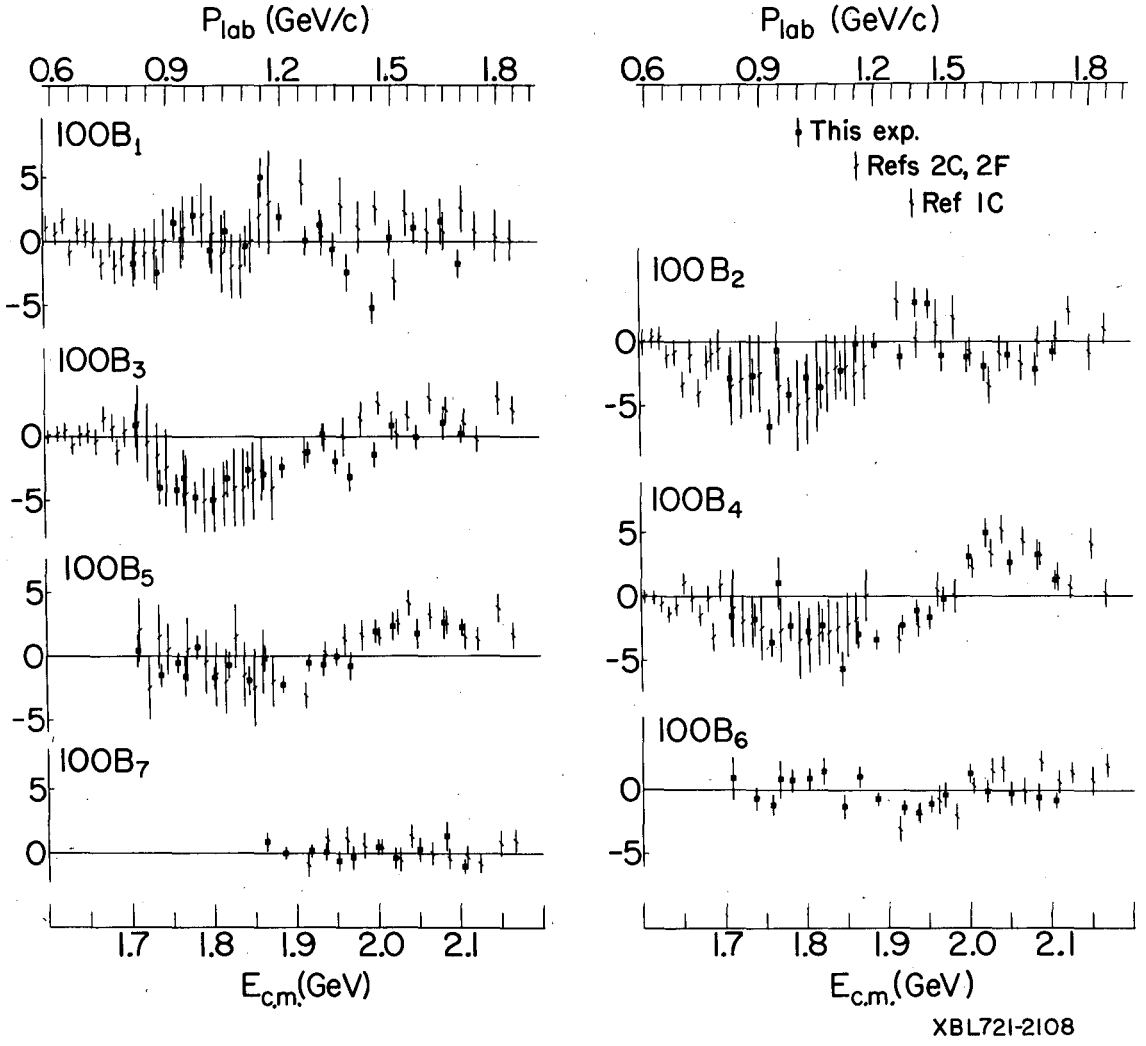
P_lab (GeV/c)
0.6
0.9
1.2
1.5
1.8
100B1
100B3
100B5
100B7
5
0
-5
1.7
1.8
1.9
2.0
2.1
E_c.m.(GeV)
This exp.
Refs 2C, 2F
Ref 1C
100B2
100B4
100B6
XBL721-2108

Fig. 9

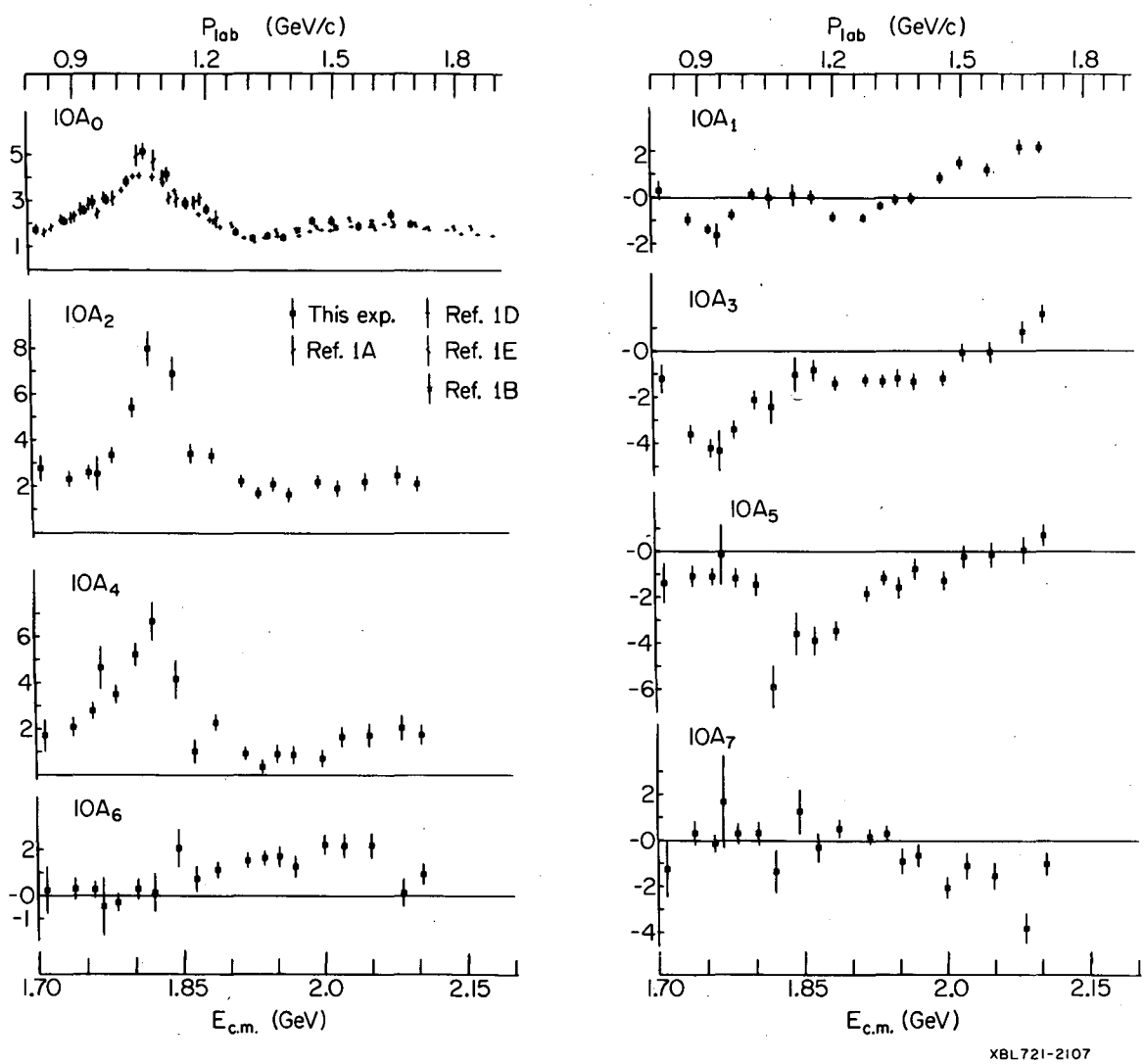
P_lab (GeV/c)
0.9
1.2
1.5
1.8
10A0
10A1
10A2
10A3
10A4
10A5
10A6
10A7
This exp.
Ref. 1A
Ref. 1D
Ref. 1E
Ref. 1B
1.70
1.85
2.0
2.15
E_c.m. (GeV)
XBL721-2107

Fig. 10

LEGAL NOTICE

This report was prepared as an account of work sponsored by the United States Government. Neither the United States nor the United States Atomic Energy Commission, nor any of their employees, nor any of their contractors, subcontractors, or their employees, makes any warranty, express or implied, or assumes any legal liability or responsibility for the accuracy, completeness or usefulness of any information, apparatus, product or process disclosed, or represents that its use would not infringe privately owned rights.

TECHNICAL INFORMATION DIVISION
LAWRENCE BERKELEY LABORATORY
UNIVERSITY OF CALIFORNIA
BERKELEY, CALIFORNIA 94720